An Efficient Analysis of Scattering From Randomly Distributed Obstacles Using an Accurate Recursive Aggregated Centered T-Matrix Algorithm

Marvin Degen, *Graduate Student Member, IEEE*, Vakhtang Jandieri, *Senior Member, IEEE*, Benedikt Sievert, *Member, IEEE*, Jan Taro Svejda, *Member, IEEE*, Andreas Rennings, *Member, IEEE*, and Daniel Erni, *Member, IEEE*

***Abstract*— An efficient recursive aggregated centered transition matrix (T-matrix) algorithm (RACTMA) to analyze electromagnetic scattering from many randomly distributed obstacles is derived. The algorithm is based on the scatterer-centered T-matrix formalism and is accelerated using the aggregation concept—unlike other approaches—without violating the addition theorems. An analytical derivation for the T-matrix of multiple cylinders together with the details of the computational complexity are given. Scattering by more than 3000 noncircular elements is numerically studied, and the results for the scattered fields are compared with those obtained by a well-established recursive T-matrix algorithm and, to demonstrate a proper convergence, the results are also compared with a commercial finite element method (FEM)-based full-wave solver. The results show a perfect agreement and demonstrate a high computational efficiency of the proposed semianalytical formalism for normal and oblique incidences. The optical theorem and the reciprocity relationship are fully satisfied confirming the accuracy and numerical stability of the approach.**

***Index Terms*— Electromagnetic analysis, scattering, transition matrix (T-matrix) method.**

I. Introduction

ELECTROMAGNETIC wave scattering by many particles has been extensively studied due to its wide practical relevance in the manipulation of electromagnetic waves [1], [2], [3], [4], [5], [6], in biomedical engineering [7], [8], [9], and in geophysics [10]. In the case of scattering elements which are distributed in a domain that exceeds several wavelengths, conventional numerical approaches such as the finite element method (FEM) [11] or the finite-difference time-domain (FDTD) [12] method require long computation time due to the whole domain of interest that must be spatially discretized and surrounded by an absorbing boundary condition to fulfill the radiation condition. This circumstance can be overcome using the method of moments (MoM) [13] which, however, is computationally costly for a large number of unknowns. Using the multilevel fast multipole algorithm (MLFMA) [14] or butterfly-based algorithm [15], the computational complexity of the iterative solver in the MoM can be significantly reduced.

A common disadvantage of all the algorithms described so far is that due to the involved iterative inversion schemes, they are only apt to calculate the scattered field for a fixed incident field, and thus, for the case of a changing incidence field, many computations must be repeated. Recently in [16], a butterfly-based algorithm with small complexity for the direct inversion of a large impedance matrix in the MoM to overcome this limitation has been proposed which, however, requires nontrivial operations in the analysis of different incidences and deals with a large factor suppressed in the $O(\cdot)$ notation of the complexity [17]. As a generalization of the Mie-solution [18], the transition matrix (T-matrix) method can overcome these limitations, since it is entirely based on the series expansions into eigenfunctions of the wave equation and the system of equations are solved using a direct method. Once the T-matrix is known, the scattered field for each incidence is obtained by a simple matrix multiplication. The T-matrix method deals not only with nonspherical particles [19], [20], [21], multilayered particles [22], [23], and multiple particle systems [21], [24], [25], [26], [27], [28], [29], [30], [31], [32] but also provides physical insight into the mutual interactions between the particles [24]. Thus, the T-matrix method is addressed and developed in many publications [33] and also covered in electromagnetic theory textbooks [34]. Following the standard procedure of electromagnetic scattering by multielement systems [24], using the translation matrices that take into account the multiple interaction process between the particles, a set of linear equations for the unknown scattering coefficients of each individual element is derived. One of the efficient techniques to deal with the large system of equations is the recursive method [21], [27], [28], [29], [30], [31], [32] which avoids the inversion of large matrices and reduces the computational complexity. A recursive T-matrix algorithm (RTMA) has been developed in [27] and [28]. Its computational complexity has been further decreased by developing the recursive aggregated T-matrix algorithm (RATMA),

Manuscript received 17 March 2023; revised 1 August 2023; accepted 7 September 2023. Date of publication 25 September 2023; date of current version 20 December 2023. This work was supported in part by the Deutsche Forschungs-Gemeinschaft (DFG, German Research Foundation) under Project 287022738—CRC/TRR 196 MARIE (Project M03). *(Corresponding author: Marvin Degen.)*

The authors are with the Laboratory for General and Theoretical Electrical Engineering (ATE), University of Duisburg-Essen, 45141 Essen, Germany, and also with CENIDE–Center for Nanointegration Duisburg-Essen, 47048 Duisburg, Germany (e-mail: marvin.degen@unidue.de).

Color versions of one or more figures in this article are available at https://doi.org/10.1109/TAP.2023.3316792.

Digital Object Identifier 10.1109/TAP.2023.3316792

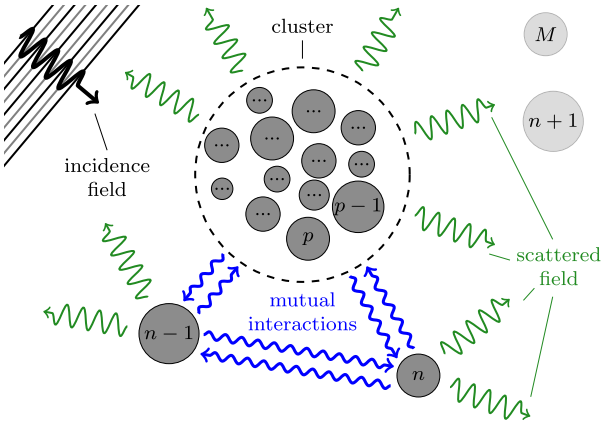

Fig. 1. Working principle of the proposed RACTMA to solve an M-cylinder scattering problem. The figure shows the state after the $(n-1)$th recursion: the mutual interactions between cylinders $1,\ldots,n$ are considered. The algorithm is accelerated due to the aggregation of $p \leq n$ obstacles in a cluster (surrounded by the dashed line) which are properly chosen to avoid a violation of the addition theorems. In the following recursions, mutual interactions with the remaining $M-n$ cylinders (grayed out) are taken into account and the cluster is extended. The details are given in Section III.

which aggregates all the particles and derives the T-matrix of a single equivalent scatterer representing the multiple element system [29]. However, the RATMA poses severe restrictions on the geometry of the problem [35, p. 158], due to the restricted area of validity of the translation matrices (Graf addition theorem in the 2-D case) and their poorly converging behavior close to the validity limit [31]. The convergence becomes worse in the case of large particles when higher order spatial harmonics are required. Therefore, large particles must be spatially discretized and considered as a cluster of many small particles [28], [29], which leads to a substantial increase in the computational costs [31]. Since the aggregation concept introduces additional, numerically evaluated indirect translations, the convergence slows further. Although it may be overcome by applying windowing [30], the latter influences the solution in converging regions [31]. A modified recursive algorithm is proposed to deal with larger particles without spatial discretization [31]; however, as it is pointed out in [36], this algorithm still involves indirect translations leading to the aforementioned numerical instabilities. To avoid the use of numerically evaluated indirect translations and thus, to increase the numerical stability, a recursive centered T-matrix algorithm (RCTMA) based on the scatterer-centered T-matrix [37] has been developed [32]. However, this advantage is at the expense of computational efficiency since the number of involved matrices considerably increases [38].

In this article, the aggregation concept of the RATMA [29] is combined with the RCTMA [32] to propose a recursive aggregated centered T-matrix algorithm (RACTMA), which shows a high accuracy and significantly reduces the computational complexity. The basic working principle to solve an M-cylinder scattering problem is shown in Fig. 1. A similar approach is given in [39] and [40]. However, due to clear and rigorous mathematical derivations, special attention is paid to the validity limits of the addition theorems and their violations resulting in a tailored a priori criterion for the particles which can be aggregated in each step without loss of accuracy [see (19a) and (19b) and an improved criterion in (22a) and (22b)]. This is mandatory for the fast and accurate scattering analysis. Following these rules, our numerical results are in a perfect agreement with the reference solution (RCTMA), which is, due to the lack of such rules, not the case in [39]. A general advantage of the RACTMA is that it is free of any restrictions on the position of the scattering elements (except that they must not intersect each other) and does not require a discretization of them. Thus, the RACTMA can be used to efficiently solve the scattering problem from many irregularly arranged particles with different material and geometrical characteristics without violating the addition theorems.

Although the proposed algorithm can be applied to 3-D geometries, the structures under consideration here are geometrically invariant in the direction of infinite extension, namely, along the z-axis in Fig. 2, illuminated under normal and oblique incidences. In the numerical analysis (cf. Section IV), we consider over 3000 noncircular cylinders, and the scattering characteristics show an excellent agreement with those obtained based on the RCTMA, but with substantially increased computational efficiency. Specifically, in the numerical examples, RACTMA is up to 17.5× faster than RCTMA. We assume our semianalytical approach to be more exact than the results obtained using purely numerical methods; however, we also compare the results obtained using the RACTMA with independent results based on the FEM using COMSOL Multiphysics [41] to demonstrate a proper convergence of the obtained results where, for two selected examples, the FEM was up to 22× slower than the RACTMA.

This article is organized as follows. In Section II, the basic concept of the T-matrix approach including involved translation matrices and their limitations are formulated and the RTMA, RATMA, and RCTMA are briefly reviewed. The formalism of our proposed RACTMA is given in Section III, including discussions about violations of the addition theorems and an analytical determination of the computational complexity. In Section IV, two different geometries are analyzed proving the efficiency and accuracy of the proposed formalism.

A time-harmonic dependence $e^{j\omega t}$ is assumed but not explicitly written throughout this article.

II. T-Matrix Formulation for a Cluster of Cylinders

The transition matrix, which is usually referred as the T-matrix, is based on the expansion of the electromagnetic fields into a series of solutions of the wave equation and relates the amplitudes of the scattered to the incident fields. The cylinders with permittivity ε_i, permeability μ_i, and radius of the circumscribing circle ρ_i, where $i = 1, 2, \ldots, M$, and M is the total number of cylinders, are located in a background medium with the permittivity ε_s and the permeability μ_s (cf. Fig. 2). The local polar coordinate attached to each cylinder is (r_i, α_i) and $d_{i,j}$ is the separation distance between the ith and jth cylinders, respectively. The cylinders are uniform and infinitely long along the z-axis. Thus, the scattering problem is reduced to a 2-D problem with a leading E_z field for TM-polarization and H_z field for TE-polarization, separately.

To avoid confusion, in this section we only depict circular cylinders. However, they can be replaced with noncircular cylinders (see the numerical examples) having the same circumscribing radius. Besides, we derive the expressions assuming a normal incidence of the waves. Taking into account the hybrid waves, an extension to the oblique incidence case is straightforward, as it is formulated in the Appendix.

For the simplest case of an isolated single cylinder illuminated under the normal incidence, using a complete orthogonal set of cylindrical wave functions, the incident u_{inc} and the scattered u_{scat} fields are expanded around the cylinder axis in terms of cylindrical space harmonics in the following form:

$$u_{\text{inc}}(r,\alpha) = \boldsymbol{\Phi}^T \cdot \boldsymbol{a} = \sum_{\nu=-\infty}^{\infty} a_\nu J_\nu(k_s r)\mathrm{e}^{\mathrm{j}\nu\alpha} \tag{1a}$$

$$u_{\text{scat}}(r,\alpha) = \boldsymbol{\Psi}^T \cdot \boldsymbol{p} = \sum_{\nu=-\infty}^{\infty} p_\nu H_\nu^{(2)}(k_s r)\mathrm{e}^{\mathrm{j}\nu\alpha} \tag{1b}$$

where $\boldsymbol{\Phi} = [J_\nu(k_s r)\mathrm{e}^{\mathrm{j}\nu\alpha}]$, $\boldsymbol{\Psi} = [H_\nu^{(2)}(k_s r)\mathrm{e}^{\mathrm{j}\nu\alpha}]$, $J_\nu(k_s r)$ and $H_\nu^{(2)}(k_s r)$ are the Bessel function of the first kind and the Hankel function of the second kind, respectively, $k_s = \omega\sqrt{\varepsilon_s \mu_s}$ is the wavenumber of the surrounding medium, ω is the angular frequency, $\boldsymbol{a} = [a_\nu]$ and $\boldsymbol{p} = [p_\nu]$ are the amplitude vectors of the incident and scattered fields, respectively, and the superscript T denotes a transpose of the vectors. We denote the standing cylindrical and outgoing cylindrical waves by the column vectors $\boldsymbol{\Phi}$ and $\boldsymbol{\Psi}$, respectively. Here, the polar radius coordinate r is the distance from the center of the isolated single cylinder to the observation point, and the angle coordinate α is the observation angle from the positive x-axis.

The calculation of the T-matrix relating the scattered field and the incident field amplitudes through the expression

$$\boldsymbol{p} = \mathbf{T} \cdot \boldsymbol{a} \tag{2}$$

can be carried out numerically using different methods [19], [20], [21]. For a circular cylinder, the T-matrix, which is then a diagonal matrix, can be easily obtained in closed form by applying the boundary condition on the surface of the cylinder [22].

For the multicylinder system, we have to take into account the multiple interactions of the fields scattered from the individual cylinders. Although more than 3000 cylinders are considered in the numerical examples (cf. Section IV), a two-element system with the ith and jth circular cylinders is shown in Fig. 2. Interactions between the cylinders are addressed by treating, besides the external excitation, the scattered waves from the ith cylinder (jth cylinder) as equivalent incident waves impinging on the jth cylinder (ith cylinder) using the translation matrices for the cylindrical wave functions. Using the local cylindrical coordinate systems (r_i, α_i) and (r_j, α_j) whose origins are located at the center of the cylinders, the translation matrices $\mathbf{A}^{i,j}$ and $\mathbf{C}^{i,j}$ transform $\boldsymbol{\Phi}_j$ and $\boldsymbol{\Psi}_j$ into $\boldsymbol{\Phi}_i$ and $\boldsymbol{\Psi}_i$ according to Graf's addition theorem in the following

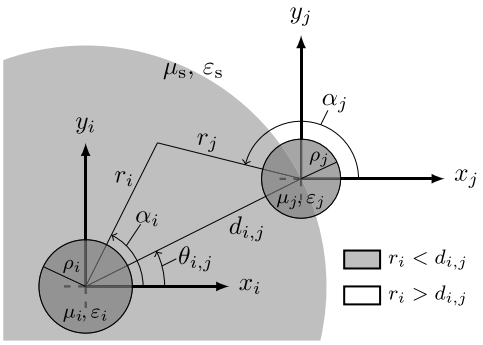

Fig. 2. Circular cylinders with permittivity ε_m, permeability μ_m, and radius ρ_m, where $(m = 1, \ldots i, j, \ldots, M)$, are located in a background medium with the permittivity ε_s and the permeability μ_s, and M is the total number of cylinders. The local coordinate systems of only two cylinders and the interaction between them are shown. The local polar coordinate system attached to each cylinder is (r_i, α_i) and (r_j, α_j), and $d_{i,j}$ is the separation distance between the ith and jth cylinders. The validity regions of the translation matrices in (3b) and (3c) together with (4a) and (4b) are marked in white and gray.

form [42, p. 361]:

$$\boldsymbol{\Phi}_j^T = \boldsymbol{\Phi}_i^T \cdot \mathbf{A}^{i,j} \quad \forall\, r_i \tag{3a}$$

$$\boldsymbol{\Psi}_j^T = \boldsymbol{\Psi}_i^T \cdot \mathbf{A}^{i,j} \quad \forall\, r_i > d_{i,j} \tag{3b}$$

$$\boldsymbol{\Psi}_j^T = \boldsymbol{\Phi}_i^T \cdot \mathbf{C}^{i,j} \quad \forall\, r_i < d_{i,j} \tag{3c}$$

with

$$A_{\mu\nu}^{i,j} = J_{\mu-\nu}(k_s\, d_{i,j})\, \mathrm{e}^{-\mathrm{j}(\mu-\nu)\theta_{i,j}} \tag{4a}$$

$$C_{\mu\nu}^{i,j} = H_{\mu-\nu}^{(2)}(k_s\, d_{i,j})\, \mathrm{e}^{-\mathrm{j}(\mu-\nu)\theta_{i,j}} \tag{4b}$$

where $\boldsymbol{\Phi}_i = [J_\nu(k_s r_i)\mathrm{e}^{\mathrm{j}\nu\alpha_i}]$ and $\boldsymbol{\Psi}_i = [H_\nu^{(2)}(k_s r_i)\mathrm{e}^{\mathrm{j}\nu\alpha_i}]$. The validity regions of the translation matrices given by (3b) and (3c) together with (4a) and (4b) are marked in white and gray in Fig. 2. Applying the boundary conditions on the surfaces of both the cylinders, a set of linear equations for the unknown scattering amplitudes of each individual cylinder can be derived and the matrix equation is solved with a suitable truncation of the matrix size. As the system of equations is ill-conditioned and the number of unknowns increases with the number of cylinders, there exists a variety of recursive algorithms to treat the multiple elements system, such as the RTMA [28], the RATMA [29], and the RCTMA [32]. In all these algorithms, the sizes of the matrices to be inverted are much smaller compared with those in a direct solution of the system of equations. First, we briefly describe all these three algorithms, and then, we propose an RACTMA including the rules for an aggregation scheme (cf. Section III), which is the fundamental result of this work.

A. Recursive T-Matrix Algorithm

The RTMA calculates the matrix $\mathbf{T}_{\{n+1\}}^j \;\forall\, j \le (n+1)$ which relates the scattered $\boldsymbol{p}_j$ to the incident $\boldsymbol{a}_j$ amplitudes of the jth cylinder $\boldsymbol{p}_j = \mathbf{T}_{\{n+1\}}^j \cdot \boldsymbol{a}_j$ taking into account the multiple interaction between all $(n+1)$ cylinders. It is recursively calculated from $\mathbf{T}_{\{n\}}^j$ in the following form:

$$\mathbf{T}_{\{n+1\}}^j = \mathbf{T}_{\{n\}}^j \cdot \left[\mathbf{I} + \mathbf{C}^{j,n+1} \cdot \mathbf{T}_{\{n+1\}}^{n+1} \cdot \mathbf{A}^{n+1,j}\right] \tag{5}$$

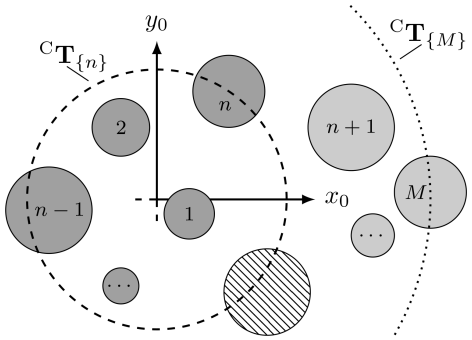

Fig. 3. Aggregated T-matrix ${}^{\mathrm{C}}\mathbf{T}_{\{n\}}$ (${}^{\mathrm{C}}\mathbf{T}_{\{M\}}$) of a system with a total number of n (dark gray) and M (dark gray and light gray) cylinders. The index 0 indicates the (local) coordinate system of the aggregate. The scattered field calculated by ${}^{\mathrm{C}}\mathbf{T}_{\{n\}}$ (${}^{\mathrm{C}}\mathbf{T}_{\{M\}}$) is valid outside the dashed (dotted) circles, respectively. The hatched cylinder cannot be analyzed using the RATMA due to a violation of the addition theorems (see Section III).

with

$$\mathbf{T}^{n+1}_{\{n+1\}} = \left[\mathbf{I} - \mathbf{T}_{n+1}\cdot\sum_{j=1}^{n}\mathbf{C}^{n+1,j}\cdot\mathbf{T}^{j}_{\{n\}}\cdot\mathbf{C}^{j,n+1}\right]^{-1} \cdot\mathbf{T}_{n+1}\cdot\left[\mathbf{I} + \sum_{j=1}^{n}\mathbf{C}^{n+1,j}\cdot\mathbf{T}^{j}_{\{n\}}\cdot\mathbf{A}^{j,n+1}\right] \tag{6}$$

where $\mathbf{T}_{n+1}$ is the T-matrix of the single $(n+1)$th cylinder in isolation, and $\mathbf{I}$ is a unit matrix. The translation matrices $\mathbf{A}$ and $\mathbf{C}$ are given in a similar form as in (4a) and (4b). Note that in the RTMA the inverse matrix is used only in (6). For the details, the interested reader is referred to [28]. Since the RTMA formalism involves indirect translations (cf. Section III-A), the truncation of the translation matrices leads to numerical instabilities, in particular for large scatterers [31] which are not spatially discretized [28].

B. Recursive Aggregated T-Matrix Algorithm

An aggregated T-matrix ${}^{\mathrm{C}}\mathbf{T}_{\{n\}}$ relates the amplitudes $\boldsymbol{a}_0$ of the incidence field to the amplitudes $\boldsymbol{p}_{0,\{n\}}$ of the scattered field for a cluster composed of n cylinders $\boldsymbol{p}_{0,\{n\}} = {}^{\mathrm{C}}\mathbf{T}_{\{n\}}\cdot\boldsymbol{a}_0$, where index 0 refers to the local coordinate system of the cluster. The geometry of the problem is shown in Fig. 3. In the RATMA formalism, the T-matrix of each cylinder is transformed into the coordinate with the origin at the center of the cluster and combined. Hence, ${}^{\mathrm{C}}\mathbf{T}_{\{n\}}$ acts as an equivalent T-matrix of an obstacle (dashed line in Fig. 3) with the same scattering characteristic as all the aggregated cylinders, and it is calculated using the translation matrices given in (3a) and (3c) by the following relationship:

$${}^{\mathrm{C}}\mathbf{T}_{\{n\}} = \sum_{j=1}^{n}\mathbf{A}^{0,j}\cdot\mathbf{T}^{j}_{\{n\}}\cdot\mathbf{A}^{j,0}. \tag{7}$$

The calculation of the aggregated T-matrix for $(n+1)$ cylinders ${}^{\mathrm{C}}\mathbf{T}_{\{n+1\}}$ is now reduced to a simple two-scatterer problem, namely, the first scatterer (dashed line in Fig. 3) with all n cylinders is characterized by the T-matrix ${}^{\mathrm{C}}\mathbf{T}_{\{n\}}$ and the second single scatterer is characterized by the T-matrix $\mathbf{T}_{n+1}$ of the $(n+1)$th cylinder in isolation. Applying (7), a simple recurrence relationship can be easily obtained

$${}^{\mathrm{C}}\mathbf{T}_{\{n+1\}} = {}^{\mathrm{C}}\mathbf{T}_{\{n\}} + {}^{\mathrm{C}}\mathbf{T}_{\{n\}}\cdot\mathbf{C}^{0,n+1}\cdot\mathbf{T}^{n+1}_{\{n+1\}}\cdot\mathbf{A}^{n+1,0} + \mathbf{A}^{0,n+1}\cdot\mathbf{T}^{n+1}_{\{n+1\}}\cdot\mathbf{A}^{n+1,0} \tag{8}$$

where

$$\mathbf{T}^{n+1}_{\{n+1\}} = \left[\mathbf{I} - \mathbf{T}_{n+1}\cdot\mathbf{C}^{n+1,0}\cdot{}^{\mathrm{C}}\mathbf{T}_{\{n\}}\cdot\mathbf{C}^{0,n+1}\right]^{-1}\cdot\mathbf{T}_{n+1} \cdot\left[\mathbf{I} + \mathbf{C}^{n+1,0}\cdot{}^{\mathrm{C}}\mathbf{T}_{\{n\}}\cdot\mathbf{A}^{0,n+1}\right]. \tag{9}$$

A detailed derivation of the algorithm is shown in [29]. Following [29], the cylinders must be sorted a priori with an increasing separation distance of their center to the center of the aggregate. However, as pointed out in Section III-A, there must be severe restrictions on the geometry not to violate the addition theorems, which prevents the hatched cylinder in Fig. 3 being added to the cluster characterized by ${}^{\mathrm{C}}\mathbf{T}_{\{n\}}$.

The computational time for solving a 2-D scattering problem with M cylinders using the RATMA scales with $O(M^2)$ [29] compared with $O(\sqrt{M^5})$ of the RTMA [28]. Due to the application of (7) and the restrictions of the translation matrices [cf. (3a)–(3c)], the aggregated T-matrices ${}^{\mathrm{C}}\mathbf{T}_{\{n\}}$ and ${}^{\mathrm{C}}\mathbf{T}_{\{M\}}$ can only be used to calculate the scattered field outside the aggregate (indicated by the dashed and dotted lines, respectively, in Fig. 3), whereas the RTMA can be used to calculate the scattered field everywhere outside the cylinder. However, this limitation of the RATMA can be overcome using the backward recursion procedure shown in [29] at the expense of an additional computational effort.

C. Recursive Centered T-Matrix Algorithm

The RCTMA can be used to calculate the scatterer-centered $\mathbf{T}^{k}_{j,\{n\}}$-matrix recursively. It is a matrix that calculates the scattered field of the jth cylinder (field is viewed from the local coordinate system of the jth cylinder) caused by the incident field impinging on the kth cylinder (field is viewed from the local coordinate system of the kth element) when multiple interactions between all the cylinders $1,\ldots,n$ are taken into account. The scatterer-centered $\mathbf{T}^{k}_{j,\{n\}}$-matrix is related to the $\mathbf{T}^{j}_{\{n\}}$-matrix used in the RTMA formalism [37]

$$\mathbf{T}^{j}_{\{n\}} = \sum_{k=1}^{n}\mathbf{T}^{k}_{j,\{n\}}\cdot\mathbf{A}^{k,j}. \tag{10}$$

Unlike the RTMA and the RATMA, an advantage of this approach is that we can avoid indirect translations, and hence: 1) the sizes of all the scatterer-centered $\mathbf{T}^{k}_{j,\{n\}}$-matrices and the translation matrices are much smaller and 2) the addition theorems are not violated [32]. A detailed derivation of the RCTMA is given in [32].

The recursion formulae in the RCTMA formalism written in the form

$$\mathbf{T}^{n+1}_{n+1,\{n+1\}} = \left[\mathbf{I} - \mathbf{T}_{n+1} \cdot \sum_{\ell=1}^{n}\sum_{m=1}^{n} \mathbf{C}^{n+1,\ell} \cdot \mathbf{T}^{m}_{\ell,\{n\}} \cdot \mathbf{C}^{m,n+1}\right]^{-1} \cdot \mathbf{T}_{n+1} \quad (11a)$$

$$\mathbf{T}^{k}_{n+1,\{n+1\}} = \mathbf{T}^{n+1}_{n+1,\{n+1\}} \cdot \sum_{\ell=1}^{n} \mathbf{C}^{n+1,\ell} \cdot \mathbf{T}^{k}_{\ell,\{n\}} \quad (11b)$$

$$\mathbf{T}^{n+1}_{j,\{n+1\}} = \sum_{m=1}^{n} \mathbf{T}^{m}_{j,\{n\}} \cdot \mathbf{C}^{m,n+1} \cdot \mathbf{T}^{n+1}_{n+1,\{n+1\}} \quad (11c)$$

$$\mathbf{T}^{k}_{j,\{n+1\}} = \mathbf{T}^{k}_{j,\{n\}} + \sum_{m=1}^{n} \mathbf{T}^{m}_{j,\{n\}} \cdot \mathbf{C}^{m,n+1} \cdot \mathbf{T}^{k}_{n+1,\{n+1\}} \quad (11d)$$

can be directly derived by substituting (10) into (6) and (5). Although only (11a) involves a matrix inversion and the costs to determine all the matrices (11a)–(11d) are reduced due to smaller matrix sizes, the disadvantage of the RCTMA compared with the RTMA and the RATMA is the number of matrices to be determined in each recursion step. Using the RACTMA derived in Section III, this circumstance is significantly mitigated.

III. Efficient T-Matrix Algorithm for a Cluster of Randomly Distributed Cylinders

In Section II, we briefly reviewed three well-known Recursive T-Matrix algorithms, which allow calculating the scattered field of a cluster of cylinders. In this section, we show that only the RCTMA can be applied to a composite of multiple cylinders without posing severe restrictions on their positions but at the expense of an increased computational effort. We derive an efficient RACTMA, which can be considered as a combination of the RCTMA using scatterer-centered T-matrices and the aggregation concept in the RATMA resulting in: 1) a substantially increased computational efficiency and 2) avoiding violations of the addition theorems.

A. Violation of the Addition Theorems

The translation matrices, which appear in Graf's addition theorem and are expressed through the cylindrical Hankel and Bessel functions in (3a) to (3c), show convergence and yield accurate results only in a certain validity region (cf. Fig. 2). We distinguish two types of violations of the addition theorems:

Type 1: violations due to indirect translations between unaggregated cylinders;

Type 2: violations due to a field evaluation inside a cluster after its aggregation.

For an illustrative demonstration, a geometry of a configuration with only three cylinders is shown in Fig. 4. The indirect translations in the RTMA formalism are written in the following form [32]:

$$\mathbf{C}^{k,\ell} = \mathbf{A}^{k,j} \cdot \mathbf{C}^{j,\ell} \quad \forall\, d_{j,\ell} > d_{j,k} + \rho_k \quad (12a)$$

$$\mathbf{C}^{j,\ell} = \mathbf{A}^{j,k} \cdot \mathbf{C}^{k,\ell} \quad \forall\, d_{k,\ell} > d_{j,k} + \rho_j. \quad (12b)$$

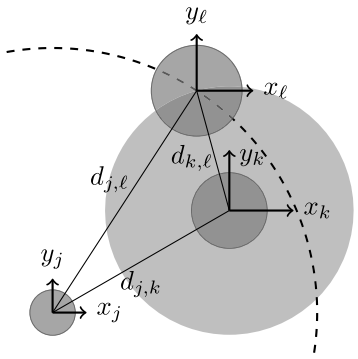

Fig. 4. Geometry of a three-cylinder configuration. Outside the gray highlighted region (dashed circle), field expansions involving a translation matrix $\mathbf{C}^{k,\ell}$ ($\mathbf{C}^{j,\ell}$) violate the addition theorems.

An indirect translation (12a) can only be applied if the kth cylinder lies completely inside a circle of radius $d_{j,\ell}$ centered at the jth cylinder, i.e., $d_{j,\ell} > d_{j,k} + \rho_k$. It can be easily shown that the RTMA violates the addition theorems in general. In the geometry illustrated in Fig. 4, the kth cylinder lies inside the dashed circle, and thus, the addition theorem is not violated when the translation matrix $\mathbf{C}^{j,\ell}$ is applied. However, the jth cylinder is located outside the gray highlighted area, in a region where a field expansion involving the translation matrix $\mathbf{C}^{k,\ell}$ violates the addition theorem. Hence, an indirect translation (12b) violates the addition theorem (violation *Type 1*) which may lead to erroneous results for the T-matrices. Due to the recursive character of the RTMA, further steps will lead to an error propagation.

Since the RATMA is derived from the RTMA involving further indirect translations, it suffers from the same *Type 1* violations of the addition theorems as the RTMA. In addition, the RATMA involves *Type 2* violations: in each step of calculation, the problem is reduced to multiple interactions between two obstacles (cf. Section II-B) and the boundary conditions should be correctly applied on the surfaces of these obstacles. This inherently requires that the scattered field of the first (second) obstacle can be expanded into cylindrical waves viewed from the coordinate system of the second (first) obstacle, which must be valid on the surface of the second (first) obstacle. Since the approach uses a translation of type (3b) in (7), the determined scattered field using the cluster T-matrix can be evaluated only outside the circle marked by the dashed line in Fig. 3. Thus, the $(n+1)$th cylinder is not allowed to intersect the dashed circle in Fig. 3, which yields severe restrictions on the geometry [35, p. 158] as, e.g., the hatched cylinder in Fig. 3 cannot be taken into account using the RATMA.

In the RCTMA, violations of *Type 1* are avoided as the formalism does not involve any indirect translations due to the use of scatterer-centered T-matrices. In addition, since no aggregation is involved in the RCTMA, violations of *Type 2* are also omitted. However, these improvements come at the expense of computational efficiency. Particularly, as it will be shown in Section III-D, the computational complexity to solve the scattering problem of M identical cylinders using the RCTMA is of $O(M^3)$.

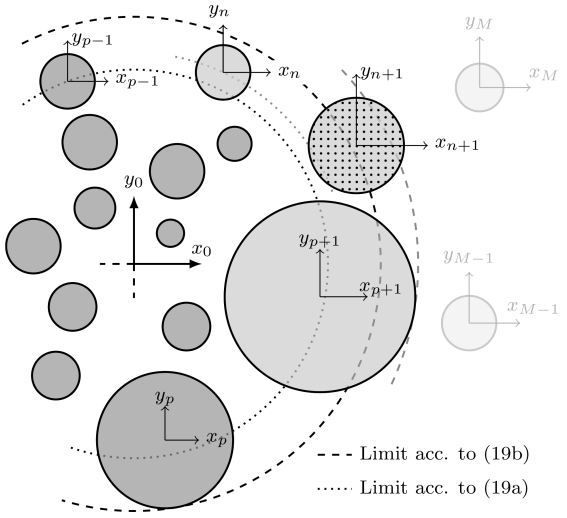

Fig. 5. Geometry of an M-cylinder configuration solved using the RACTMA. During the nth calculation step, $\{p\}$ (dark gray) cylinders are aggregated in a cluster [cf. (15a)–(15c)], whereas the others are characterized by the scatterer-centered T-matrices. The $(p+1)$th and nth cylinders cannot be added to the cluster due to a violation of the addition theorems (the origin of the $(n+1)$th cylinder lays inside the gray dashed circle and the gray dotted circle intersects with the $(n+1)$th cylinder). During the following calculation steps, the cluster is extended based on (20a)–(20c) taking into the cylinders that do not violate (19a) and (19b).

B. Recursive Aggregated Centered T-Matrix Algorithm

To solve a scattering problem using the RTMA and the RATMA, severe restrictions are posed on the geometries to prevent a violation of the addition theorems (cf. Section III-A). In addition, electrically large cylinders cannot be considered as one single scatterer but should be spatially discretized [28], [31]. These limitations are circumvented in the RCTMA formalism, but at the expense of computational efficiency as the number of matrices to be determined using the RCTMA equals to the squared number of matrices in the RTMA. Here, we propose an RACTMA, which uses the elements of the RCTMA but with substantially increased computational efficiency due to the aggregation approach. Namely, the computational complexity of the RACTMA compared with the RCTMA is reduced from $O(M^3)$ to $O(M^2)$; the details are given in Section III-D. In [39] and [40], a comparable method is derived, but without rules for the scatterers to be aggregated in each recurrence step (an a posteriori brute-force ansatz was used in [39]). Here, due to the rigorous derivations, we introduce an a priori criterion [cf. (19a) and (19b)] and an improved a priori criterion [cf. (22a) and (22b)] ensuring the nonviolation of the addition theorems to identify these scatterers. The criteria are essential for efficient and accurate scattering analysis.

Fig. 5 shows an M-cylinder configuration to be solved with the RACTMA during the nth computational step. Unlike the RATMA formalism, where all n cylinders are aggregated before the nth step, in the RACTMA only $p \leq n$ (dark gray in Fig. 5) of them are aggregated. As in the RCTMA formalism, the RACTMA calculates the scatterer-centered T-matrices recursively. However, in the RACTMA the centered T-matrices also characterize the aggregated elements. Taking into account the multiple interactions between the n cylinders (set of the dark and light gray cylinders in Fig. 5), the cluster-centered T-matrices $\mathbf{T}^{\{p\}}_{\{p\},\{n\}}$ ($\mathbf{T}^{k}_{\{p\},\{n\}}$) determined in Section II-C relate the amplitudes $\boldsymbol{a}_0$ ($\boldsymbol{a}_k$) of an incident field to the amplitudes $\boldsymbol{p}^{\{p\}}_{\{p\},\{n\}}$ ($\boldsymbol{p}^{k}_{\{p\},\{n\}}$) of a scattered field for the cluster composed of $\{p\}$ cylinders due to the field impinging on the cluster (on the kth cylinder) in the following form:

$$\boldsymbol{p}^{\{p\}}_{\{p\},\{n\}} = \mathbf{T}^{\{p\}}_{\{p\},\{n\}} \cdot \boldsymbol{a}_0 \tag{13a}$$

$$\boldsymbol{p}^{k}_{\{p\},\{n\}} = \mathbf{T}^{k}_{\{p\},\{n\}} \cdot \boldsymbol{a}_k. \tag{13b}$$

Accordingly, the $(n-p)$ unaggregated obstacles are characterized by their scatterer-centered T-matrices $\mathbf{T}^{k}_{j,\{n\}}$ $(p < j,\, k \leq n)$ and $\mathbf{T}^{\{p\}}_{j,\{n\}}$, where the former are the scatterer-centered T-matrices used in the RCTMA formalism and the latter relates the amplitudes $\boldsymbol{a}_0$ of the incidence field to the amplitudes $\boldsymbol{p}^{\{p\}}_{j,\{n\}}$ of the scattered field for the jth cylinder due to the field impinging on $\{p\}$ aggregated obstacles

$$\boldsymbol{p}^{\{p\}}_{j,\{n\}} = \mathbf{T}^{\{p\}}_{j,\{n\}} \cdot \boldsymbol{a}_0. \tag{14}$$

After several mathematical manipulations, the cluster-centered T-matrices in (13a) and (13b) and the scatterer-centered T-matrix in (14) can be expressed through the scatterer-centered T-matrix $\mathbf{T}^{k}_{j,\{n\}}$ using (3a) and (3b) in the following form:

$$\mathbf{T}^{\{p\}}_{\{p\},\{n\}} = \sum_{j=1}^{p}\sum_{k=1}^{p} \mathbf{A}^{0,j} \cdot \mathbf{T}^{k}_{j,\{n\}} \cdot \mathbf{A}^{k,0} \tag{15a}$$

$$\mathbf{T}^{k}_{\{p\},\{n\}} = \sum_{j=1}^{p} \mathbf{A}^{0,j} \cdot \mathbf{T}^{k}_{j,\{n\}} \quad \forall\ p < k \leq n \tag{15b}$$

$$\mathbf{T}^{\{p\}}_{j,\{n\}} = \sum_{k=1}^{p} \mathbf{T}^{k}_{j,\{n\}} \cdot \mathbf{A}^{k,0} \quad \forall\ p < j \leq n. \tag{15c}$$

Following the procedure in Section III-A, one can easily show that for an indirect translation of the form $\mathbf{C}^{k,\ell} = \mathbf{C}^{k,j} \cdot \mathbf{A}^{j,\ell}$, where $\mathbf{C}^{k,j}$ appears in (3c) and $\mathbf{A}^{j,\ell}$ appears in (3b), to omit the violation of the addition theorems, the following condition must be fulfilled:

$$\mathbf{C}^{k,\ell} = \mathbf{C}^{k,j} \cdot \mathbf{A}^{j,\ell} \quad \forall\ d_{j,\ell} < d_{j,k} - \rho_k. \tag{16}$$

Substituting (15a)–(15c) into (11a)–(11d) and using the indirect translations (12a) and (16), the following set of new four recurrence equations is obtained:

$$\begin{aligned}\mathbf{T}^{n+1}_{n+1,\{n+1\}} = \Bigg[&\mathbf{I} - \mathbf{T}_{n+1} \cdot \mathbf{C}^{n+1,0} \cdot \mathbf{T}^{\{p\}}_{\{p\},\{n\}} \cdot \mathbf{C}^{0,n+1} \\ &- \mathbf{T}_{n+1} \cdot \sum_{j=p+1}^{n} \left(\mathbf{C}^{n+1,j} \cdot \mathbf{T}^{\{p\}}_{j,\{n\}} \cdot \mathbf{C}^{0,n+1}\right) \\ &- \mathbf{T}_{n+1} \cdot \sum_{k=p+1}^{n} \left(\mathbf{C}^{n+1,0} \cdot \mathbf{T}^{k}_{\{p\},\{n\}} \cdot \mathbf{C}^{k,n+1}\right) \\ &- \mathbf{T}_{n+1} \cdot \sum_{j=p+1}^{n}\sum_{k=p+1}^{n} \left(\mathbf{C}^{n+1,j} \cdot \mathbf{T}^{k}_{j,\{n\}} \cdot \mathbf{C}^{k,n+1}\right)\Bigg]^{-1} \\ &\cdot \mathbf{T}_{n+1}\end{aligned} \tag{17a}$$

$$\begin{aligned}\mathbf{T}^{k}_{n+1,\{n+1\}} = &\mathbf{T}^{n+1}_{n+1,\{n+1\}} \cdot \mathbf{C}^{n+1,0} \cdot \mathbf{T}^{k}_{\{p\},\{n\}} \\ &+ \mathbf{T}^{n+1}_{n+1,\{n+1\}} \cdot \sum_{j=p+1}^{n} \left(\mathbf{C}^{n+1,j} \cdot \mathbf{T}^{k}_{j,\{n\}}\right)\end{aligned} \tag{17b}$$

$$\mathbf{T}^{k}_{j,\{n+1\}} = \mathbf{T}^{k}_{j,\{n\}} + \mathbf{T}^{\{p\}}_{j,\{n\}} \cdot \mathbf{C}^{0,n+1} \cdot \mathbf{T}^{k}_{n+1,\{n+1\}} + \sum_{\ell=p+1}^{n} \left(\mathbf{T}^{\ell}_{j,\{n\}} \cdot \mathbf{C}^{\ell,n+1}\right) \cdot \mathbf{T}^{k}_{n+1,\{n+1\}} \tag{17c}$$

$$\mathbf{T}^{n+1}_{j,\{n+1\}} = \mathbf{T}^{\{p\}}_{j,\{n+1\}} \cdot \mathbf{C}^{0,n+1} \cdot \mathbf{T}^{n+1}_{n+1,\{n+1\}} + \sum_{\ell=p+1}^{n} \left(\mathbf{T}^{\ell}_{j\{n\}} \cdot \mathbf{C}^{\ell,n+1}\right) \cdot \mathbf{T}^{n+1}_{n+1,\{n+1\}} \tag{17d}$$

where

$$p < k \leq n \text{ or } k = \{p\}$$
$$p < j \leq n \text{ or } j = \{p\}.$$

Comparing (15a)–(15c) and (17a)–(17d), it is obvious that (17a)–(17d) involve numerically evaluated indirect translations of the following form:

$$\mathbf{C}^{n+1,j} = \mathbf{C}^{n+1,0} \cdot \mathbf{A}^{0,j}, \quad \text{for } 1 \leq j \leq p \tag{18a}$$
$$\mathbf{C}^{k,n+1} = \mathbf{A}^{k,0} \cdot \mathbf{C}^{0,n+1}, \quad \text{for } 1 \leq k \leq p. \tag{18b}$$

Thus, to avoid a violation of the addition theorems [restrictions in (12a) and (16)], one can derive two rules that the $\{p\}$ aggregated cylinders must follow:

$$d_{0,j} < d_{0,k} - \rho_k \quad \forall\ 1 \leq j \leq p \text{ and } n < k \leq M \tag{19a}$$
$$d_{0,k} > d_{0,j} + \rho_j \quad \forall\ 1 \leq j \leq p \text{ and } n < k \leq M. \tag{19b}$$

The cylinders are properly chosen during each calculation step based on (19a) and (19b) which are implemented in the numerical code. Here, (19a) ensures that before the nth calculation step, no cylinder $k > n$ must lay inside or intersect the circle (dotted line in Fig. 5) centered at the origin of the cluster with radius

$$\max_{1\leq j\leq p}\left(d_{0,j}\right)$$

, and (19b) ensures that the origins of cylinders $k > n$ must lay outside the circle (dashed line in Fig. 5) around the aggregated cylinders with radius

$$\max_{1\leq j\leq p}\left(d_{0,k} + \rho_k\right).$$

It is easy to see that (19a) and (19b) are the same if all the cylinders are of equal size.

After each calculation step, the cluster is extended by t cylinders which are properly selected based on (19a) and (19b). After several mathematical manipulations, the extended cluster-centered and the scatterer-centered T-matrices can be derived from (15a) to (15c) according to

$$\mathbf{T}^{k}_{\{p+t\},\{n\}} = \mathbf{T}^{k}_{\{p\},\{n\}} + \sum_{j=p+1}^{p+t} \mathbf{A}^{0,j} \cdot \mathbf{T}^{k}_{j,\{n\}} \quad \forall\ p+t < k \leq n \tag{20a}$$

$$\mathbf{T}^{\{p+t\}}_{j,\{n\}} = \mathbf{T}^{\{p\}}_{j,\{n\}} + \sum_{k=p+1}^{p+t} \mathbf{T}^{k}_{j,\{n\}} \cdot \mathbf{A}^{k,0} \quad \forall\ p+t < j \leq n \tag{20b}$$

TABLE I
TRUNCATION NUMBER OF THE MATRICES INVOLVED IN THE RACTMA FORMALISM (17A)–(17D) AND (20A)–(20C)

Matrix:	$\mathbf{T}_j$	$\mathbf{T}^{k}_{j,\{n\}}$	$\mathbf{T}^{k}_{\{p\},\{n\}}$	$\mathbf{T}^{\{p\}}_{j,\{n\}}$	$\mathbf{T}^{\{p\}}_{\{p\},\{n\}}$
Trunc.:	$\kappa \times \kappa$	$\kappa \times \kappa$	$\Lambda \times \kappa$	$\kappa \times \Lambda$	$\Lambda \times \Lambda$

Matrix:	$\mathbf{C}^{n+1,0}$	$\mathbf{C}^{0,n+1}$	$\mathbf{C}^{n+1,j}$	$\mathbf{C}^{k,n+1}$
Trunc.:	$\kappa \times \Lambda$	$\Lambda \times \kappa$	$\kappa \times \kappa$	$\kappa \times \kappa$

Matrix:	$\mathbf{A}^{k,0}$	$\mathbf{A}^{0,j}$
Trunc.:	$\kappa \times \Lambda$	$\Lambda \times \kappa$

$$\mathbf{T}^{\{p+t\}}_{\{p+t\},\{n\}} = \mathbf{T}^{\{p\}}_{\{p\},\{n\}} + \sum_{k=p+1}^{p+t} \mathbf{T}^{k}_{\{p\},\{n\}} \cdot \mathbf{A}^{k,0} + \sum_{j=p+1}^{p+t} \mathbf{A}^{0,j} \cdot \mathbf{T}^{\{p\}}_{j,\{n\}} + \sum_{j=p+1}^{p+t}\sum_{k=p+1}^{p+t} \mathbf{A}^{0,j} \cdot \mathbf{T}^{k}_{j,\{n\}} \cdot \mathbf{A}^{k,0}. \tag{20c}$$

Note that (17a)–(17d) and (20a)–(20c) (a similar set of equations can be found in [39] and [40]) together with the proposed a priori criterion for the aggregation in (19a) and (19b) are the key expressions for the RACTMA.

C. Improved Criterion for the Aggregation

All the translation matrices and T-matrices in the RACTMA must be truncated, which yields a truncation error. Following [43, Lemma 3.1], the truncation errors for the standing cylindrical and outgoing cylindrical wave expansions—ξ_Φ and ξ_Ψ, respectively—fulfill the following inequalities:

$$\xi_\Phi < c\left(\frac{R_\Phi}{\widetilde{R}_\Phi}\right)^{N_\Phi}, \quad R_\Phi < \widetilde{R}_\Phi \tag{21a}$$

$$\xi_\Psi < c\left(\frac{\widetilde{R}_\Psi}{R_\Psi}\right)^{N_\Psi}, \quad R_\Psi > \widetilde{R}_\Psi \tag{21b}$$

where c is a finite constant, $\widetilde{R}_\Phi$ ($\widetilde{R}_\Psi$) is the radius of a circle that lays in the region where the standing (outgoing) cylindrical wave function expansion is valid, R_Φ and R_Ψ correspond to the radius of observation points of the respective fields, and $N_\Phi > k_s \widetilde{R}_\Phi$, $N_\Psi > k_s \widetilde{R}_\Psi$ are the orders of truncation of the standing cylindrical and outgoing cylindrical wave expansions.

In (19a) and (19b), we ensured that no addition theorems are violated. However, the obstacles can approach the invalid area arbitrarily close, and when following (21a) and (21b), the truncation error increases. Thus, to keep the RACTMA numerically stable and avoid the use of a computational expensive high cluster-centered T-matrix truncation number, an additional distance $\delta \geq 0$ is introduced in (19a) and (19b) yielding the following two modified rules:

$$d_{0,j} < d_{0,k} - \rho_k - \delta \quad \forall\ 1 \leq j \leq p \text{ and } n < k \leq M \tag{22a}$$
$$d_{0,k} > d_{0,j} + \rho_j + \delta \quad \forall\ 1 \leq j \leq p \text{ and } n < k \leq M. \tag{22b}$$

TABLE II
COMPUTATIONAL COMPLEXITY OF (17A)–(17D) AND (20A)–(20C) WITH RESPECT TO n. THE OVERALL COMPLEXITY OF THE nTH RECURSION SCALES ACCORDING TO THE LARGEST TOTAL COMPLEXITY OF ALL ROWS

Eq.	j	k	Complexity per Call		No. of Calls	Total Complexity	
(17a)	–	–	$O(\Lambda^2+(n-p)+(n-p)^2)$	$=O(n)$	1	$O(n)$	
(17b)	–	$\{p\}$	$O(\Lambda^2+(n-p)+\Lambda)$	$=O(n)$	1	$O(n)$	
(17b)	–	$p<k\leq n$	$O(\Lambda+(n-p))$	$=O(\sqrt{n})$	$(n-p)$	$O((n-p)\sqrt{n})$	$=O(n)$
(17c)	$\{p\}$	$\{p\}$	$O(\Lambda^2)$	$=O(n)$	1	$O(n)$	
(17c)	$\{p\}$	$p<k\leq n$	$O(\Lambda)$	$=O(\sqrt{n})$	$(n-p)$	$O((n-p)\sqrt{n})$	$=O(n)$
(17c)	$p<j\leq n$	$\{p\}$	$O(\Lambda+(n-p)+\Lambda)$	$=O(\sqrt{n})$	$(n-p)$	$O((n-p)\sqrt{n})$	$=O(n)$
(17c)	$p<j\leq n$	$p<k\leq n$	$O(1)$	$=O(1)$	$(n-p)^2$	$O((n-p)^2)$	$=O(n)$
(17d)	$\{p\}$	–	$O(\Lambda)$	$=O(\sqrt{n})$	1	$O(\sqrt{n})$	
(17d)	$p<j\leq n$	–	$O(\Lambda)$	$=O(\sqrt{n})$	$(n-p)$	$O((n-p)\sqrt{n})$	$=O(n)$
(20a)	–	$p+t<k\leq n$	$O(\Lambda)$	$=O(\sqrt{n})$	$(n-p-t)$	$O((n-p-t)\sqrt{n})$	$=O(n)$
(20b)	$p+t<j\leq n$	–	$O(\Lambda)$	$=O(\sqrt{n})$	$(n-p-t)$	$O((n-p-t)\sqrt{n})$	$=O(n)$
(20c)	–	–	$O(\Lambda^2)$	$=O(n)$	1	$O(n)$	
					Overall Complexity n-th recursion:	$\underline{O(n)}$	

The value of δ strongly depends on the geometry of the problem. It is properly chosen to guarantee accurate results and is given in Section IV-B for the specific geometries investigated there.

D. Computational Complexity

From the analysis of Section III-B follows that due to the proposed aggregation scheme in the RACTMA, the total number of scatterer-centered and cluster-centered T-matrices to be determined during the nth computation step reduces from $(n+1)^2$ [38] (cf. (11a) to (11d)) in the RCTMA to $(n-p+2)^2$ [cf. (17a)–(17d)] in the RACTMA. However, to go deeply into the analysis of computational complexity of the RACTMA, we consider M randomly distributed identical cylinders, each having a radius ρ, as illustrated in Fig. 6. The cylinders are distributed within a circle with radius R_M and the inclusion density η, i.e., a ratio of the area covered by cylinders to the total area, is assumed to be a constant within the bounding circle. The cylinders are characterized by scatterer-centered T-matrices, whose truncation number is κ. The number of cylinders distributed within the circles having radii $d_{0,p}$ and $d_{0,n}$ is p and n, respectively.

A truncation number Λ of the translation matrices appearing in (15a)–(15c) is calculated in the following form [28]:

$$\Lambda = C\, k_s\, d_{0,p} \text{ with } C > 1 \tag{23}$$

where k_s is the wavenumber in the background medium, and C is a constant, which as a rule of thumb may vary between 1 and 5. In general, C could change in every recursion step and should be chosen properly to ensure that Λ does not exceed the truncation number of the incidence field. Consequently, the truncation numbers of all the matrices involved in the RACTMA formalism (17a)–(17d) and (20a)–(20c) are summarized in Table I. To meet the requirements of (22a) and (22b), the following equality should be fulfilled:

$$d_{0,n} = d_{0,p} + \gamma\,\rho \tag{24}$$

where $\gamma = 1+\delta/\rho$. Taking into account η, $d_{0,p}$ and $d_{0,n}$ can be expressed through p and n in the following form:

$$d_{0,p} = \frac{\rho}{\sqrt{\eta}}\sqrt{p} \tag{25a}$$

$$d_{0,n} = \frac{\rho}{\sqrt{\eta}}\sqrt{n}. \tag{25b}$$

Next, substituting (25a) and (25b) into (24), p and $d_{0,p}$ can be written as a function of n as

$$p = \eta\left(\frac{\sqrt{n}}{\sqrt{\eta}} - \gamma\right)^2 \tag{26a}$$

$$d_{0,p} = \rho\left(\frac{\sqrt{n}}{\sqrt{\eta}} - \gamma\right). \tag{26b}$$

Substituting (26b) into (23), an asymptotic behavior of Λ with respect to n can be obtained

$$\Lambda = O\left(\sqrt{n}\right). \tag{27}$$

As the scatterers are assumed to be randomly distributed, t is independent of n, and accordingly, $t = O(1)$. The computational complexity of (17a)–(17d) and (20a)–(20c) with respect to n is shown in Table II. The values in the fourth and sixth columns are obtained using (26a) and (27). The total complexity at the nth step of the RACTMA is of $O(n)$, whereas the evaluation of the RCTMA formalism is of $O(n^2)$ (cf. Section II-C).

Finally, we can conclude that since the solution of a problem with M cylinders requires $M-1$ recursions in the RACTMA and the RCTMA, the computational complexities to solve the entire problem, K_{RACTMA} and K_{RCTMA}, can be written in the following form:

$$K_{\text{RACTMA}} = O\left(\sum_{n=1}^{M-1} n\right) = O\left(M^2\right) \tag{28a}$$

$$K_{\text{RCTMA}} = O\left(\sum_{n=1}^{M-1} n^2\right) = O\left(M^3\right) \tag{28b}$$

where the second right-hand side terms are obtained using [44, (0.121.1.) and (0.121.2.)].

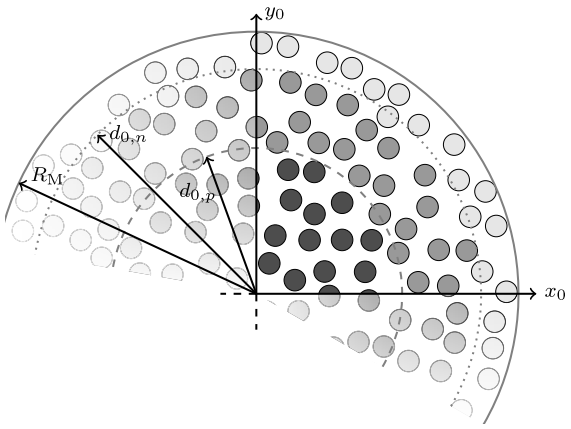

Fig. 6. M randomly distributed cylinders each having a radius ρ and a constant inclusion density within the bounding circle of radius R_M. During the nth calculation step, p (dark gray) cylinders are aggregated in a cluster of a circle with a radius $d_{0,p}$ (dashed circle). Multiple interactions between n cylinders—dark gray and medium gray—bounded by a dotted circle of radius $d_{0,n}$ are considered. The next calculation steps take into account the interaction with the $(M-n)$ light gray cylinders.

IV. Numerical Results and Discussions

To demonstrate the efficiency of the RACTMA formalism, two geometries—shown in Section IV-A—are analyzed. The developed RACTMA is implemented in a MATLAB [45] numerical code using standard double-precision arithmetic. The results are compared with those based on the RCTMA and, as an independent method, the commercial FEM solver COMSOL Multiphysics [41], although we assume results based on the semianalytical T-matrix approach to be more accurate. All the tests have been performed on an AMD Ryzen Threadripper PRO 3955WX 16-Core processor with a base clock frequency of 3.9 GHz and 245 GB of RAM.

A. Geometries Under Investigation

The first geometry depicted in Fig. 7(a) consists of M circular cylinders with the same radius ρ distributed within a circumscribing circle having a radius R_M. In the numerical analysis, up to $M = 3159$ cylinders are considered. To obtain a roughly constant inclusion density η within the circumscribing circle, all the cylinders are arranged using a modification of the Poisson disk sampling algorithm [46]. The background medium is the free space with permittivity $\varepsilon_s = \varepsilon_0$ and permeability $\mu_s = \mu_0$. The cylinders are nonpermeable ($\mu_i = \mu_0$), and approximately 20% randomly selected cylinders (hatched) are assumed as perfect electric conductors (PECs). The dielectric permittivities of the remaining cylinders randomly vary according to an equal distribution between $\varepsilon_i = 2\varepsilon_0$ and $\varepsilon_i = 10\varepsilon_0$. Plane waves are impinging on the structure, and the angle of incidence with respect to the x-axis is denoted by α_{inc}. The dotted circle of radius $R_{NF} = 1.5\,R_M$ mimics a near-field receiver, where the scattered fields are evaluated. To demonstrate that our proposed RACTMA can also be applied to the scattering analysis of a cluster of noncircular cylinders, we deformed the circular cross section of the cylinder in Fig. 7(a) with Chebyshev polynomials [cf. Fig. 7(b)–(e)]. Thus, the cross sections of Chebyshev

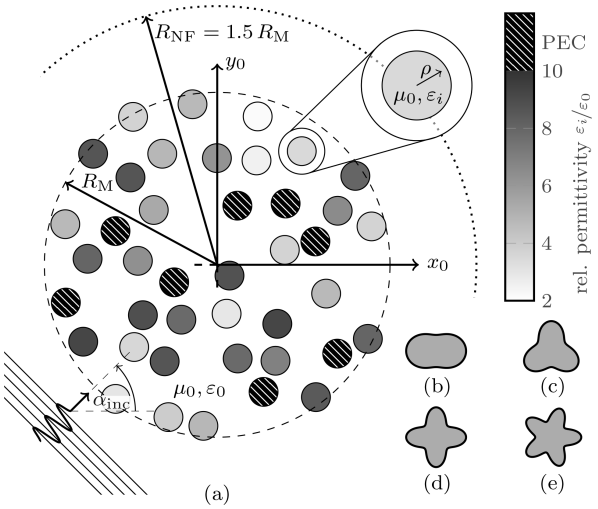

Fig. 7. (a) Cluster of M cylinders distributed within a circumscribing circle (dashed) having a radius R_M using a modification of the Poisson disk sampling algorithm. The color intensity of the ith cylinder indicates a permittivity $\varepsilon_i \in [2\varepsilon_0, 10\varepsilon_0]$, whereas the hatched cylinders are PECs. The dotted circle of radius R_{NF} shows the position of the receiver to analyze the near-field characteristics. Plane waves are impinging on the structure and α_{inc} is the angle of incidence with respect to the x-axis. (b)–(e) Cylindrical Chebyshev particles of degrees 2–5, respectively, which are also considered as scattering elements in the cluster.

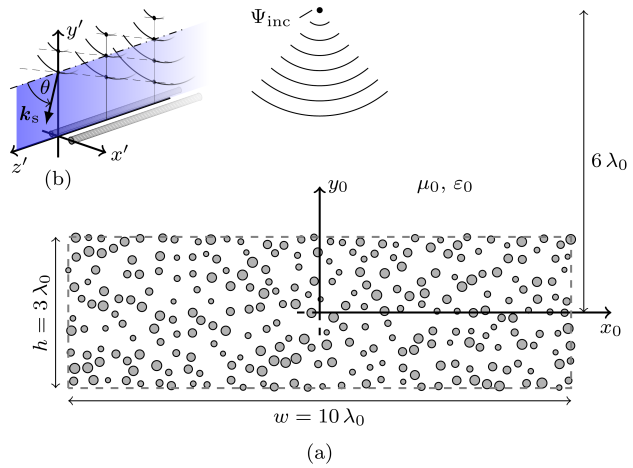

Fig. 8. (a) Cluster of M cylinders within a rectangle having a width $w = 10\lambda_0$ and a height $h = 3\lambda_0$. The radii of the cylinders are randomly varying $\rho_i \in [0.05\lambda_0, 0.1\lambda_0]$, whereas the material parameters of all the cylinders are identical, i.e., $\mu_i = \mu_0$ and $\varepsilon_i = 10\varepsilon_0$. A line source is placed at a height of $6\lambda_0$ above the center of the rectangle (b) generating waves impinging on the structure under the oblique angle θ with respect to the z-axis.

cylinders are given by the following expression:

$$r(\alpha) = (\rho - \varsigma)\left(1 + \varsigma\, \mathrm{T}_{n_0}(\cos(\alpha))\right) = (\rho - \varsigma)\left(1 + \varsigma\, \cos(n_0\,\alpha)\right) \quad (29)$$

where T_{n_0} is the Chebyshev polynomial of order n_0, ς is the deformation parameter, and ρ the radius of the smallest circumscribing circle. In the numerical example, n_0 and ς randomly vary between $2 \ldots 5$ and $0 \ldots 0.15$, respectively, ρ is identical for all the cylinders, and the permittivity is randomly varying between $\varepsilon_i = 2 \ldots 10$.

A second geometry shown in Fig. 8 is composed of $M = 270$ cylinders embedded into the free space within a

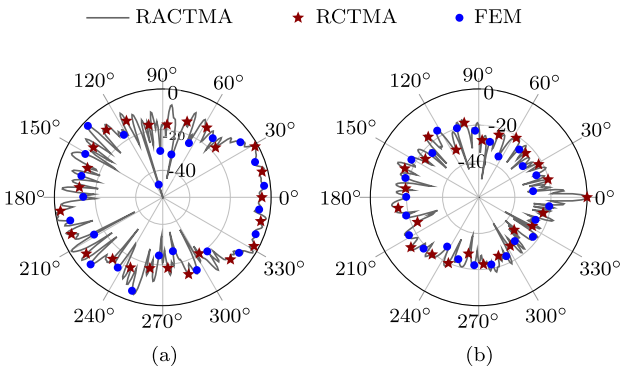

Fig. 9. Magnitude of the scattered magnetic field $\|\boldsymbol{H}\|$ (dB) for a TE-polarized plane wave incident on the structure (see Fig. 7) composed of 355 cylinders with a radius $\rho = 0.3\lambda_0$ placed within an umscribing circle of radius $R_{\mathrm{M}} = 9\lambda_0$. The magnetic field is evaluated (a) at a distance R_{NF} from the center of the cluster and (b) in the far-field region. The results are compared with those obtained based on the RCTMA and the FEM solver COMSOL Multiphysics.

umscribing rectangle (gray dashed line) having a width $w = 10\lambda_0$ and a height $h = 3\lambda_0$. Here, λ_0 is the wavelength in the free space. As in the first example, the distribution of the cylinders is given using a modification of the Poisson disk sampling algorithm. The dielectric permittivities of the cylinders are identical $\varepsilon_i = 10\varepsilon_0$, whereas the radii are randomly varying between $0.05\lambda_0$ and $0.1\lambda_0$. The TE/TM line source (magnetic/electric line current) for the excitation of the impinging cylindrical wave is placed at a height $h = 6\lambda_0$ above the center of the rectangular scatterer domain [cf. Fig. 8(a)]. The waves are impinging on the structure under the oblique angle θ with respect to the z-axis, as illustrated in Fig. 8(b).

B. Numerical Analysis

First, we study the scattering of a TE (H_z, E_x, E_y)-polarized electromagnetic wave impinging on the structure shown in Fig. 7. A number of $M = 355$ circular cylinders with a radius $\rho = 0.3\lambda_0$ are distributed within the circle having a radius $R_M = 9\lambda_0$. The magnitudes of the scattered magnetic field $\|\boldsymbol{H}\|$ at a distance $R_{\mathrm{NF}} = 1.5R_{\mathrm{M}}$ and in the far-field region are displayed in Fig. 9. The results show an excellent agreement between all the three approaches. The CPU time required to calculate the cluster T-matrix is considerably reduced from 245 s (RCTMA) to 59 s (RACTMA), whereas the CPU time required to solve the scattering problem using the FEM (including setting up the geometry and meshing) was approximately 414 s. It is important to note that the cluster T-matrix obtained using the RCTMA and the RACTMA can directly be used to determine the scattered field for all the incident fields of same frequency, which can be expanded into a cylindrical harmonics series, whereas the FEM must be repeated in case of any change in the incidence field. The truncation number N_{inc} of the series expansion of the plane wave used in the RCTMA and RACTMA is determined by the equality

$$N_{\mathrm{inc}} = 2\,k_{\mathrm{s}}\,R_{\mathrm{M}}. \tag{30}$$

The truncation number κ of the scatterer-centered T-matrices is equal to 7, whereas the truncation number of the

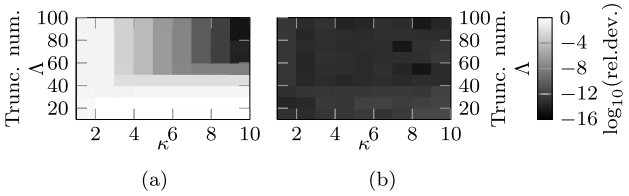

Fig. 10. Relative deviation of (a) optical theorem and (b) reciprocity relationship for different tuples of truncation numbers Λ and κ for geometry 1 composed of 158 Chebyshev cylinders with $\rho/\lambda_0 = 0.3$ and $R_{\mathrm{M}} = 6\lambda_0$ under TM-polarized plane wave illumination as a measure to control the truncation error.

cluster-centered T-matrices Λ is determined using (23) with C following the relationship:

$$C = \min\left(4,\ \frac{N_{\mathrm{inc}}}{k_{\mathrm{s}}\,d_{0,p}}\right) \tag{31}$$

and δ is chosen as $\delta = 0.5\lambda_0$. The second term in the min function in (31) limits Λ to the truncation number of the incidence field, as described in Section III-D.

Since the aggregation in the RACTMA does not violate the addition theorems, (17a)–(17d) and (20a)–(20c) are, as (11a)–(11d) for the RCTMA, in principle exact aiming both the semianalytical methods to be used as a reference solution. Thus, if the T-matrices in isolation are known, all the errors in the numerical analysis are solely caused by a limited machine precision and by the truncation order of the T-matrices and translation matrices κ and Λ, respectively. Regarding the impact of δ, we refer to Section III-C.

As a measure for the truncation error, the optical theorem—the relative deviation between the scattering cross section and the extinction cross section—can be analyzed for the cluster T-matrices because the truncation yields a loss of energy in the higher order harmonics [47]. The reciprocity relationship [22] can be analyzed as a measure for the round-off error due to the machine precision. The reciprocity relationship is the relative deviation between two differential scattering cross sections $\sigma_{\mathrm{d}}(\alpha_{\mathrm{inc}}, \alpha_0)$ and $\sigma_d(\alpha_0 + 180°, \alpha_{\mathrm{inc}} + 180°)$ at $\alpha_{\mathrm{inc}} = 0°$ and $\alpha_0 = 30°$.

The controllability of the truncation error in the RACTMA due to a proper choice of Λ and κ is demonstrated in Fig. 10. From the figure follows that the optical theorem converges to machine precision with increasing truncation numbers, while the relative deviation of the reciprocity relationship remains close to the machine precision. Here, we calculated the cluster T-matrix for the geometry 1 composed of 158 noncircular Chebyshev cylinders ($\rho/\lambda_0 = 0.3$ and $R_{\mathrm{M}} = 6\lambda_0$ with $\delta = 0.5\lambda_0$) under TM illumination for different values of Λ and κ.

The T-matrices in isolation of the Chebyshev cylinders have been precalculated following the procedure given in [21] by placing small circular cylinders with a radius of $\rho = 0.03\lambda_0$ into free space inside the virtual border of the Chebyshev cylinder so that the covered area fraction $f \approx 50\%$. The permittivity of the small circular cylinders ε_{c} is determined so that the effective permittivity of the composite given by the weighted average rule equals to that of the solid Chebyshev cylinder under consideration ε_i, i.e.,

$$\varepsilon_i = f\,\varepsilon_{\mathrm{c}} + (1 - f)\,\varepsilon_0. \tag{32}$$

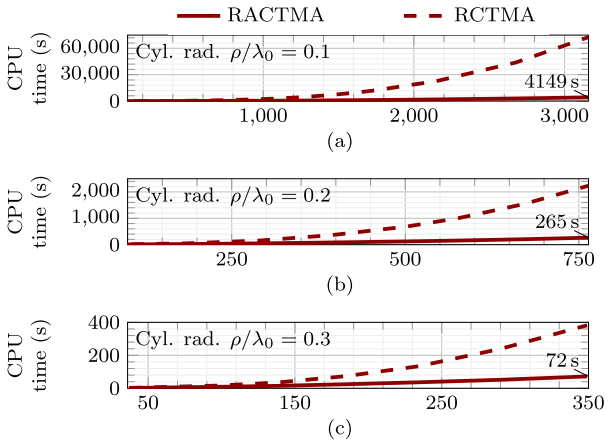

Fig. 11. CPU time to solve geometry 1 (cf. Fig. 7) composed of Chebyshev cylinders for a TM-polarized plane wave as excitation using the RCTMA and the RACTMA as a function of the number of Chebyshev cylinders M for different normalized radii circumscribing the cylinders (a) $\rho/\lambda_0 = 0.1$, (b) $\rho/\lambda_0 = 0.2$, and (c) $\rho/\lambda_0 = 0.3$. A maximum number of cylinders for their different radii is chosen so that R_{M} does not exceed $9\lambda_0$, and hence, N_{inc} is limited to 113 according to (30).

Then, the T-matrix in isolation of the noncircular cylinder equals the cluster T-matrix of the ensemble, which is efficiently calculated using the proposed RACTMA.

The superiority in computational efficiency of the RACTMA compared with the RCTMA is demonstrated in Fig. 11, where the CPU time required to determine the cluster T-matrix for the geometry 1 (see Fig. 7)—using the Chebyshev cylinders instead of the circular cylinders—for TM polarization is depicted as a function of the number of cylinders M for different normalized radii of the circumscribing circle ρ/λ_0 of the cylinders. The T-matrices in isolation of the Chebyshev cylinders have been precalculated using the procedure described in the previous paragraph.

From Fig. 11 follows that even for a moderate number M—i.e., a few hundred cylinders—RACTMA formalism is several times faster [see Fig. 11(b) and (c)] than RCTMA. The truncation number of the scatterer-centered T-matrices, κ (cf. Table I), is chosen as $\kappa = 5, 7, 8$ for $\rho = 0.1\lambda_0, 0.2\lambda_0, 0.3\lambda_0$, respectively, and Λ is determined using (23) where C is chosen according to (31). The truncation number of the incidence field and thus the truncation number of the final cluster T-matrix (which is a square matrix) is given by (30). The truncation number of the T-matrix at the last computation stage and thus that of the incidence field must be kept moderate to avoid exceeding the limit of the double-precision variables due to the highly divergent Hankel functions in particular in $\mathbf{C}^{0,n+1}$ and $\mathbf{C}^{n+1,0}$ in (17a)–(17d). Thus, we limit the number of cylinders for $\rho_0 = 0.1\lambda_0$, $\rho_0 = 0.2\lambda_0$ and $\rho_0 = 0.3\lambda_0$ to $M = 3159$, $M = 764$, and $M = 349$, respectively, which corresponds to $R_{\mathrm{M}} < 9\lambda_0$, and hence, following (30) limits N_{inc} to $N_{\mathrm{inc}} \leq 113$.

As the counterpart to Fig. 9, the magnitudes of the scattered electric field $\|\boldsymbol{E}\|$ for TM polarization and noncircular cylinders at a distance $R_{\mathrm{NF}} = 1.5\,R_{\mathrm{M}}$ and in the far-field region calculated using the RACTMA, the RCTMA and COMSOL are displayed in Fig. 12 demonstrating again an excellent agreement.

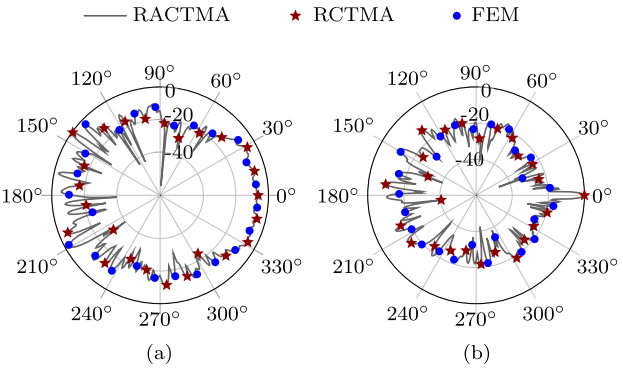

Fig. 12. Magnitude of the scattered electric field $\|\boldsymbol{E}\|$ (dB) for a TM-polarized plane wave incident on the structure (see Fig. 7) composed of 349 noncircular Chebyshev cylinders with a radius of the circumscribing circle $\rho = 0.3\lambda_0$ placed within an umscribing circle of radius $R_{\mathrm{M}} = 9\lambda_0$. The electric field is evaluated (a) at a distance R_{NF} from the center of the cluster and (b) in the far-field region. The results are compared with those obtained based on the RCTMA and the FEM solver COMSOL Multiphysics.

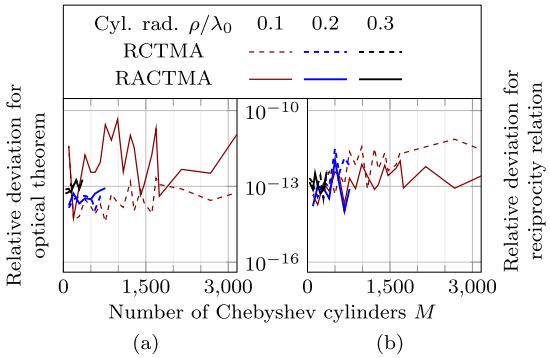

Fig. 13. (a) Relative deviation between the scattering cross section and the extinction cross section (optical theorem). (b) Relative deviation between two differential scattering cross sections $\sigma_{\mathrm{d}}(\alpha_{\mathrm{inc}}, \alpha_0)$ with $\alpha_{\mathrm{inc}} = 0^\circ$ and $\alpha_{\mathrm{inc}} = 210^\circ$ evaluated at $\alpha_0 = 30^\circ$ and $\alpha_0 = 180^\circ$ (reciprocity relationship). The number of Chebyshev cylinders is taken up to $M = 3159$ and $\rho/\lambda_0 = 0.1, 0.2,$ and 0.3. A TM-polarized plane wave impinging on geometry 1 (see Fig. 7) with Chebyshev cylinders as scattering elements is considered.

The results depicted in Fig. 13 demonstrate that both the optical theorem and reciprocity relationship are satisfied with a very high accuracy using the RCTMA and the proposed RACTMA.

The magnitudes of the scattered electric (magnetic) fields evaluated in the far-field for the TM (TE)-polarized waves [excited by the line source in the Geometry 2 in Fig. 8(a)] impinging under an oblique angle $\theta = 60^\circ$ [see Fig. 8(b)] based on the formalism of the hybrid waves given in Appendix are depicted in Fig. 14. The results show perfect agreement between the RACTMA, the RCTMA, and the FEM with COMSOL Multiphysics. The CPU time to determine the cluster T-matrix is reduced from 115 s (171 s) [RCTMA] to 40 s (49 s) [RACTMA] for TM (TE) polarization, and we used $N_{\mathrm{inc}} = 100$, $\delta = 0.5\lambda_0$, and $\kappa = 3(4)$. For comparison, the CPU time required using the FEM (including setting up the geometry and meshing) was 891 and 722 s for TM and TE polarizations, respectively. The results for the optical theorem and the reciprocity relationship are given in Table III. Here, the optical theorem is analyzed for a plane wave propagating

TABLE III

OPTICAL THEOREM AND THE RECIPROCITY RELATIONSHIP FOR THE CLUSTER T-MATRIX FOR GEOMETRY 2 (CF., FIG. 8) CALCULATED USING THE RACTMA AND THE RCTMA. FOR THE OPTICAL THEOREM, A PLANE WAVE WITH $\alpha_{\text{INC}} = 0$, WHEREAS FOR THE RECIPROCITY RELATIONSHIP, A PLANE WAVE WITH $\alpha_{\text{INC}} = 0$ AND $\alpha_{\text{INC}} = 210°$ EVALUATED AT $\alpha_0 = 30°$ AND $\alpha_0 = 180°$ IS CONSIDERED. THE RECIPROCITY RELATIONSHIP IS EVALUATED FOR CO-POLARIZATION AND CROSS-POLARIZATION, SEPARATELY

	RCTMA		**RACTMA**	
	TE	**TM**	**TE**	**TM**
recip. rel. cross-pol	$3.8 \cdot 10^{-14}$	$2.2 \cdot 10^{-14}$	$4.9 \cdot 10^{-14}$	$2.0 \cdot 10^{-14}$
recip. rel. co-pol	$2.7 \cdot 10^{-14}$	$1.5 \cdot 10^{-13}$	$1.9 \cdot 10^{-14}$	$1.3 \cdot 10^{-14}$
opt. theor.	$1.0 \cdot 10^{-14}$	$2.6 \cdot 10^{-14}$	$4.1 \cdot 10^{-13}$	$4.2 \cdot 10^{-14}$

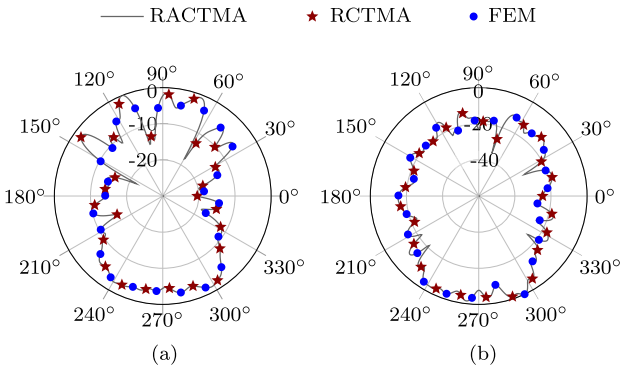

Fig. 14. Magnitude of the scattered far-field (dB) of 270 cylinders with a radius varying between $0.05\lambda_0$ and $0.1\lambda_0$ and permittivity $\varepsilon_i = 10\varepsilon_0$ distributed in a rectangular frame (cf., Fig. 8). (a) Scattered electric field $\|\boldsymbol{E}\|$ for TM-polarized incidence and (b) scattered magnetic field $\|\boldsymbol{H}\|$ for TE-polarized incidence, respectively. The background field is produced by a line source at a height of $6\lambda_0$ above the center of the cluster and the field impinges on the structure under the oblique angle $\theta = 60°$. The far-field is calculated using the RCTMA, the RATMA, and the commercial FEM solver COMSOL Multiphysics.

in the direction of the x-axis ($\alpha_{\text{inc}} = 0$), and the reciprocity relationship is analyzed for two plane waves with $\alpha_{\text{inc}} = 0$ and $\alpha_{\text{inc}} = 210°$ evaluated at $\alpha_0 = 30°$ and $\alpha_0 = 180°$ for cross- and co-polarization, separately.

V. CONCLUSION

A recursive T-matrix algorithm including a tailored a priori criterion for the aggregation has been proposed to efficiently analyze the electromagnetic scattering by many randomly distributed cylinders. The formalism does not require any discretization of the cylinders and does not pose any restrictions on their position except that the smallest circumscribing circles must not intersect. High computational efficiency is achieved as the number of matrices to be determined in each recursion step is significantly reduced due to the application of an aggregation approach, where the aggregated elements are properly chosen during each calculation step to avoid a violation of the addition theorems.

In the numerical results, the proposed algorithm was up to 17.5× faster compared with an existing T-matrix algorithm and, for two selected examples, up to 22× faster compared with the time required using the FEM. The 2-D scattering by both circular and noncircular cylinders is studied under normal and oblique incidences to demonstrate the usefulness and validity of the formalism. Its extension to 3-D geometries is straightforward. Due to the very high computational efficiency of the RACTMA, it can not only be applied to analyze the scattering of a given geometry but also in the structural optimization of structures composed of many irregularly arrange scattering elements, as it is required in the design of nonperiodic metamaterials.

APPENDIX
RACTMA FOR THE SCATTERING ANALYSIS UNDER OBLIQUE INCIDENCE

For the scattering analysis of 2-D geometries illuminated under oblique incidence with a $\mathrm{e}^{-\mathrm{j}k_z z}$ dependence along the z-direction, where $k_z = k_\mathrm{s}\cos(\theta)$ and θ is the angle with respect to the z-axis as indicated in Fig. 8(b), the existence of hybrid waves must be taken into account [34], [48]. In this case, an illuminating TM (TE) wave causes both a co-polarized TM (TE) scattered wave and a cross-polarized TE (TM) scattered wave. Thus, a coupling of both the polarizations must be considered.

As under normal incidence [cf., (1a) and (1b)], the leading E_z field for TM polarization and H_z field for TE polarization are expanded into a series of cylindrical space harmonics given by the following expressions:

$$\boldsymbol{\Phi} = [J_\nu(k_r r)\mathrm{e}^{\mathrm{j}\nu\alpha}] \tag{33a}$$

$$\boldsymbol{\Psi} = [H_\nu^{(2)}(k_r r)\mathrm{e}^{\mathrm{j}\nu\alpha}] \tag{33b}$$

where $k_r = \sqrt{k_\mathrm{s}^2 - k_z^2}$ is the propagation constant in the xy plane. To distinguish between the polarizations, $\boldsymbol{a}^\mathrm{M}$ ($\boldsymbol{a}^\mathrm{E}$) and $\boldsymbol{p}^\mathrm{M}$ ($\boldsymbol{p}^\mathrm{E}$) are the amplitude vectors of the incidence and scattered fields for TM (TE) polarization, respectively. Taking into account the scattering into co-polarized and cross-polarized waves, the amplitudes of the scattered fields are related to the amplitudes of the incident field through the following relationships:

$$\boldsymbol{p}^\mathrm{M} = \mathbf{T}^{\mathrm{MM}} \cdot \boldsymbol{a}^\mathrm{M} + \mathbf{T}^{\mathrm{ME}} \cdot \boldsymbol{a}^\mathrm{E} \tag{34a}$$

$$\boldsymbol{p}^\mathrm{E} = \mathbf{T}^{\mathrm{EE}} \cdot \boldsymbol{a}^\mathrm{E} + \mathbf{T}^{\mathrm{EM}} \cdot \boldsymbol{a}^\mathrm{M} \tag{34b}$$

where the first and second terms on the right-hand side of (34a) and (34b) represent the co-polarized and cross-polarized scattering, respectively. Equations (34a) and (34b) can be compressed into a single matrix equation

$$\begin{bmatrix} \boldsymbol{p}^\mathrm{M} \\ \boldsymbol{p}^\mathrm{E} \end{bmatrix} = \begin{bmatrix} \mathbf{T}_n^{\mathrm{MM}} & \mathbf{T}_n^{\mathrm{ME}} \\ \mathbf{T}_n^{\mathrm{EM}} & \mathbf{T}_n^{\mathrm{EE}} \end{bmatrix} \cdot \begin{bmatrix} \boldsymbol{a}^\mathrm{M} \\ \boldsymbol{a}^\mathrm{E} \end{bmatrix}. \tag{35}$$

Both the leading field components of the incidence field (E_z^{inc} and H_z^{inc}) and scattered field (E_z^{sca} and H_z^{sca}) can now be written in a similar form as in (1a) and (1b)

$$\begin{bmatrix} E_z^{\mathrm{inc}} \\ H_z^{\mathrm{inc}} \end{bmatrix} = \begin{bmatrix} \boldsymbol{\Phi}^\mathrm{T} & \mathbf{0} \\ \mathbf{0} & \boldsymbol{\Phi}^\mathrm{T} \end{bmatrix} \cdot \begin{bmatrix} \boldsymbol{a}^\mathrm{M} \\ \boldsymbol{a}^\mathrm{E} \end{bmatrix} \cdot \mathrm{e}^{-\mathrm{j}k_z z} \tag{36a}$$

$$\begin{bmatrix} E_z^{\mathrm{sca}} \\ H_z^{\mathrm{sca}} \end{bmatrix} = \begin{bmatrix} \boldsymbol{\Psi}^\mathrm{T} & \mathbf{0} \\ \mathbf{0} & \boldsymbol{\Psi}^\mathrm{T} \end{bmatrix} \cdot \begin{bmatrix} \boldsymbol{a}^\mathrm{M} \\ \boldsymbol{a}^\mathrm{E} \end{bmatrix} \cdot \mathrm{e}^{-\mathrm{j}k_z z}. \tag{36b}$$

Comparing (35) with (2) and (36a), (36b), with (1a), (1b), and (3a)–(3c), it can be easily seen that the proposed RACTMA can be directly used for the scattering analysis under the oblique incidence by following substitutions into (17a)–(17d) and (20a)–(20c):

$$\mathbf{T}_n \rightarrow \begin{bmatrix} \mathbf{T}_n^{\mathrm{MM}} & \mathbf{T}_n^{\mathrm{ME}} \\ \mathbf{T}_n^{\mathrm{EM}} & \mathbf{T}_n^{\mathrm{EE}} \end{bmatrix} \tag{37a}$$

$$\mathbf{A}^{k,\ell} \rightarrow \begin{bmatrix} \mathbf{A}^{k,\ell} & \mathbf{0} \\ \mathbf{0} & \mathbf{A}^{k,\ell} \end{bmatrix} \tag{37b}$$

$$\mathbf{C}^{k,\ell} \rightarrow \begin{bmatrix} \mathbf{C}^{k,\ell} & \mathbf{0} \\ \mathbf{0} & \mathbf{C}^{k,\ell} \end{bmatrix} \tag{37c}$$

$$\boldsymbol{p} \rightarrow \begin{bmatrix} \boldsymbol{p}^{\mathrm{M}} \\ \boldsymbol{p}^{\mathrm{E}} \end{bmatrix} \tag{37d}$$

$$\boldsymbol{a} \rightarrow \begin{bmatrix} \boldsymbol{a}^{\mathrm{M}} \\ \boldsymbol{a}^{\mathrm{E}} \end{bmatrix} \tag{37e}$$

$$k_{\mathrm{s}} \rightarrow \sqrt{k_{\mathrm{s}}^2 - k_z^2}. \tag{37f}$$

Finally, note that all the cluster-centered and scatterer-centered T-matrices in the formalism take the same form as (37a).

REFERENCES

[1] K. Yasumoto, Ed., *Electromagnetic Theory and Applications for Photonic Crystals*. Boca Raton, FL, USA: CRC Press, 2006.

[2] A. Z. Elsherbeni, M. Hamid, and G. Tian, "Iterative scattering of a Gaussian beam by an array of circular conducting and dielectric cylinders," *J. Electromagn. Waves Appl.*, vol. 7, no. 10, pp. 1323–1342, Jan. 1993.

[3] M. Polewski and J. Mazur, "Scattering by an array of conducting, lossy dielectric, ferrite and pseudochiral cylinders," *Prog. Electromagn. Res.*, vol. 38, pp. 283–310, 2002.

[4] A. Z. Elsherbeni, "A comparative study of two-dimensional multiple scattering techniques," *Radio Sci.*, vol. 29, no. 4, pp. 1023–1033, Jul. 1994.

[5] V. Jandieri and K. Yasumoto, "Analysis of scattering from a finite array of circular cylinders using a model of layered cylindrical arrays," *Opt. Commun.*, vol. 284, no. 18, pp. 4109–4113, Aug. 2011.

[6] V. Jandieri, K. Yasumoto, and Y. Liu, "Directivity of radiation of a dipole source coupled to cylindrical electromagnetic bandgap structures," *J. Opt. Soc. Amer. B, Opt. Phys.*, vol. 29, no. 9, pp. 2622–2629, Sep. 2012.

[7] J. Mroczka, D. Wysoczarski, and F. R. A. Onofri, "Optical parameters and scattering properties of red blood cells," *Opt. Appl.*, vol. 32, no. 4, pp. 691–700, Jan. 2002.

[8] S. Lambert et al., "Analysis of the structure of very large bacterial aggregates by small-angle multiple light scattering and confocal image analysis," *J. Colloid Interface Sci.*, vol. 262, no. 2, pp. 384–390, Jun. 2003.

[9] A. M. K. Nilsson, P. Alsholm, A. Karlsson, and S. Andersson-Engels, "T-matrix computations of light scattering by red blood cells," *Appl. Opt.*, vol. 37, no. 13, pp. 2735–2748, May 1998.

[10] R. A. R. Tricker, *Introduction to Meteorological Optics*. New York, NY, USA: Elsevier, 1970.

[11] G. Pelosi, R. Coccioli, and S. Sellerie, *Quick Finite Elements for Electromagnetic Waves*, 2nd ed. Norwood, MA, USA: Artech House, 2009.

[12] A. Taflove and S. C. Hagness, *Computational Electrodynamics: The Finite-Difference Time-Domain Method*, 3rd ed. Norwood, MA, USA: Artech House, 2005.

[13] R. F. Harrington, *Field Computation by Moment Methods*. Piscataway, NJ, USA: IEEE Press, 1993.

[14] W. C. Chew, J.-M. Jin, E. Michielssen, and J. Song, Eds., *Fast and Efficient Algorithms in Computational Electromagnetics*. Norwood, MA, USA: Artech House, 2006.

[15] E. Michielssen and A. Boag, "A multilevel matrix decomposition algorithm for analyzing scattering from large structures," *IEEE Trans. Antennas Propag.*, vol. 44, no. 8, pp. 1086–1093, Aug. 1996.

[16] H. Guo, Y. Liu, J. Hu, and E. Michielssen, "A butterfly-based direct integral-equation solver using hierarchical LU factorization for analyzing scattering from electrically large conducting objects," *IEEE Trans. Antennas Propag.*, vol. 65, no. 9, pp. 4742–4750, Sep. 2017.

[17] X.-W. Huang and X.-Q. Sheng, "On the theoretical and practical numerical performance of matrix-decomposition-based fast direct solvers," in *Proc. Photon. Electromagn. Res. Symp. Fall (PIERS Fall)*, Xiamen, China, Dec. 2019, pp. 361–369.

[18] G. Mie, "Contributions to the optics of turbid media, particularly of colloidal metal solutions," *Ann. Phys.*, vol. 330, no. 3, pp. 377–445, 1908.

[19] P. C. Waterman, "Matrix formulation of electromagnetic scattering," *Proc. IEEE*, vol. 53, no. 8, pp. 805–812, Aug. 1965.

[20] M. Ganesh and S. C. Hawkins, "Three dimensional electromagnetic scattering T-matrix computations," *J. Comput. Appl. Math.*, vol. 234, no. 6, pp. 1702–1709, Jul. 2010.

[21] W. C. Chew, L. Gurel, Y.-M. Wang, G. Otto, R. L. Wagner, and Q. H. Liu, "A generalized recursive algorithm for wave-scattering solutions in two dimensions," *IEEE Trans. Microw. Theory Techn.*, vol. 40, no. 4, pp. 716–723, Apr. 1992.

[22] H. Toyama, K. Yasumoto, and T. Iwasaki, "Electromagnetic scattering from a dielectric cylinder with multiple eccentric cylindrical inclusions," *Prog. Electromagn. Res.*, vol. 40, pp. 113–129, 2003.

[23] A. A. Kishk, R. P. Parrikar, and A. Z. Elsherbeni, "Electromagnetic scattering from an eccentric multilayered circular cylinder," *IEEE Trans. Antennas Propag.*, vol. 40, no. 3, pp. 295–303, Mar. 1992.

[24] B. Peterson and S. Ström, "T matrix for electromagnetic scattering from an arbitrary number of scatterers and representations of E(3)," *Phys. Rev. D, Part. Fields*, vol. 8, no. 10, pp. 3661–3678, Nov. 1973.

[25] K. A. Fuller and G. W. Kattawar, "Consummate solution to the problem of classical electromagnetic scattering by an ensemble of spheres. I: Linear chains," *Opt. Lett.*, vol. 13, no. 2, pp. 90–92, Feb. 1988.

[26] K. A. Fuller and G. W. Kattawar, "Consummate solution to the problem of classical electromagnetic scattering by an ensemble of spheres. II: Clusters of arbitrary configuration," *Opt. Lett.*, vol. 13, no. 12, pp. 1063–1065, Dec. 1988.

[27] W. C. Chew, "An N^2 algorithm for the multiple scattering solution of N scatterers," *Microw. Opt. Technol. Lett.*, vol. 2, no. 11, pp. 380–383, Nov. 1989.

[28] Y. M. Wang and W. C. Chew, "An efficient algorithm for solution of a scattering problem," *Microw. Opt. Technol. Lett.*, vol. 3, no. 3, pp. 102–106, Mar. 1990.

[29] W. C. Chew and Y. M. Wang, "A fast algorithm for solution of a scattering problem using a recursive aggregate τ matrix method," *Microw. Opt. Technol. Lett.*, vol. 3, no. 5, pp. 164–169, May 1990.

[30] W. C. Chew, Y. M. Wang, and L. Gürel, "Recursive algorithm for wave-scattering solutions using windowed addition theorem," *J. Electromagn. Waves Appl.*, vol. 6, no. 11, pp. 1537–1560, Jan. 1992.

[31] A. Sahin and E. L. Miller, "Recursive T-matrix methods for scattering from multiple dielectric and metallic objects," *IEEE Trans. Antennas Propag.*, vol. 46, no. 5, pp. 672–678, May 1998.

[32] B. Stout, J.-C. Auger, and J. Lafait, "A transfer matrix approach to local field calculations in multiple-scattering problems," *J. Mod. Opt.*, vol. 49, no. 13, pp. 2129–2152, Nov. 2002.

[33] M. I. Mishchenko, G. Videen, V. A. Babenko, N. G. Khlebtsov, and T. Wriedt, "T-matrix theory of electromagnetic scattering by particles and its applications: A comprehensive reference database," *J. Quantum Spectrosc. Radiat. Transf.*, vol. 88, pp. 357–406, Aug. 2004.

[34] W. C. Chew, *Waves and Fields in Inhomogeneous Media*. Piscataway, NJ, USA: IEEE Press, 1995.

[35] M. I. Mishchenko, L. D. Travis, and A. A. Lacis, *Scattering, Absorption, and Emission of Light by Small Particles*, 3rd ed. Cambridge, U.K.: Cambridge Univ. Press, 2002.

[36] C. Meiners, J. Psilopoulos, and A. F. Jacob, "Determining the scattered field of dense particles using recursive algorithms," *Microw. Opt. Technol. Lett.*, vol. 40, no. 6, pp. 523–529, Mar. 2004.

[37] D. W. Mackowski and M. I. Mishchenko, "Calculation of the T matrix and the scattering matrix for ensembles of spheres," *J. Opt. Soc. Amer. A, Opt. Image Sci.*, vol. 13, no. 11, pp. 2266–2278, Nov. 1996.

[38] J.-C. Auger and B. Stout, "A recursive centered T-matrix algorithm to solve the multiple scattering equation: Numerical validation," *J. Quant. Spectrosc. Radiat. Transf.*, vols. 79–80, pp. 533–547, Jun. 2003.

[39] W. C. Chew and C. C. Lu, "The recursive aggregate interaction matrix algorithm for multiple scatterers," *IEEE Trans. Antennas Propag.*, vol. 43, no. 12, pp. 1483–1486, Dec. 1995.

[40] L. Gurel and W. C. Chew, "Fast direct (noniterative) solvers for integral-equation formulations of scattering problems," in *Proc. IEEE Antennas Propag. Soc. Int. Symp.*, Jun. 1998, pp. 298–301.
[41] COMSOL Multiphysics. *COMSOL Multiphysics (6.0)*. Accessed: Mar. 15, 2023. [Online]. Available: https://comsol.com
[42] G. N. Watson, *A Treatise on the Theory of Bessel Functions*, 2nd ed. Cambridge, U.K.: Cambridge Univ. Press, 1966.
[43] V. Rokhlin, "Rapid solution of integral equations of scattering theory in two dimensions," *J. Comput. Phys.*, vol. 86, no. 2, pp. 414–439, Feb. 1990.
[44] I. S. Gradshteĭn and I. M. Ryzhik, *Table of Integrals, Series, and Products*, 7th ed., A. Jeffrey and D. Zwillinger, Eds. Burlington, MA, USA: Academic, 2007.
[45] The MathWorks. *MATLAB. (R2022a)*. Accessed: Mar. 15, 2023. [Online]. Available: https://mathworks.com
[46] R. Bridson, "Fast Poisson disk sampling in arbitrary dimensions," in *Proc. ACM SIGGRAPH Sketches*. New York, NY, USA: Association for Computing Machinery, 2007, p. 22.
[47] P. R. Siqueira and K. Sarabandi, "T-matrix determination of effective permittivity for three-dimensional dense random media," *IEEE Trans. Antennas Propag.*, vol. 48, no. 2, pp. 317–327, Feb. 2000.
[48] V. Jandieri, K. Yasumoto, and Y.-K. Cho, "Rigorous analysis of electromagnetic scattering by cylindrical EBG structures," *Prog. Electromagn. Res.*, vol. 121, pp. 317–342, 2011.

Marvin Degen (Graduate Student Member, IEEE) was born in Speyer, Germany, in 1997. He received the B.Eng. degree in electrical engineering from Baden-Wuerttemberg Cooperative State University, Mannheim, Germany, in 2019, and the M.Sc. degree in electrical engineering and information technology from the University of Duisburg-Essen, Duisburg, Germany, in 2022.

From 2019 to 2021, he worked as a Planning Engineer for energy infrastructure projects. Since 2022, he has been a member of the Laboratory of General and Theoretical Electrical Engineering, University of Duisburg-Essen. His research interests include theoretical and computational electromagnetics and its application in the manipulation of electromagnetic waves.

Vakhtang Jandieri (Senior Member, IEEE) received the D.Eng. degree in computer science and communication engineering from Kyushu University, Fukuoka, Japan, in 2006.

From 2007 to 2010, he was with Kumamoto University, Kumamoto, Japan, as a Post-Doctoral Japanese Society for Promotion of Science (JSPS) Fellow. He was a Visiting Professor with the School of Electronics Engineering and Computer Science, Kyungpook National University, Daegu, Republic of Korea, from 2010 to 2013; the Nanotechnology Center, Technical University of Ostrava, Ostrava, Czech Republic, in 2015; and the Department of Engineering, Roma Tre University, Rome, Italy, in 2015. He is currently with the Laboratory for General and Theoretical Electrical Engineering (ATE), Faculty of Engineering, and the Center for Nanointegration Duisburg-Essen (CENIDE), University of Duisburg-Essen, Duisburg, Germany. His research interests are in electromagnetic wave theory, and analytical and numerical techniques on microwave and optical photonic crystal devices.

Dr. Jandieri is a Senior Member of OSA. He was a recipient of the Paper Prize from the Institute of Electrical Engineers of Japan (IEEJ) in 2004, the URSI Young Scientist Award in 2010, and two Fulbright Awards at the University of Illinois at Urbana-Champaign, USA, from 2015 to 2016, and Pennsylvania State University, USA, in 2021. He was also a recipient of the Alexander von Humboldt Award at the University of Duisburg-Essen from 2016 to 2018.

Benedikt Sievert (Member, IEEE) was born in Krefeld, Germany. He received the B.Sc. and M.Sc. degrees in electrical engineering/high-frequency systems from the University of Duisburg-Essen, Duisburg, Germany, in 2017 and 2019, respectively.

Since 2017, he has been a member of the Laboratory of General and Theoretical Electrical Engineering, University of Duisburg-Essen. His research interests include mm-wave on-chip antennas, electromagnetic metamaterials, and theoretical and computational electromagnetics.

Jan Taro Svejda (Member, IEEE) received the B.Sc. degree in electrical engineering from the University of Applied Sciences, Düsseldorf, Germany, in 2008, and the M.Sc. and Dr.-Ing. degrees in electrical engineering and information technology from the University of Duisburg-Essen, Duisburg, Germany, in 2013 and 2019, respectively, for his research work in the field of X-nuclei-based magnetic resonance imaging.

He is currently working as a Research Assistant with the Department of General and Theoretical Electrical Engineering, University of Duisburg-Essen, where he is involved in teaching several lectures and courses mainly in the field of electrical engineering. His general research interests include all aspects of theoretical and applied electromagnetics, currently focusing on medical applications, electromagnetic metamaterials, and scientific computing methods.

Andreas Rennings (Member, IEEE) received the Dipl.-Ing. and Dr.-Ing. degrees from the University of Duisburg-Essen, Duisburg, Germany, in 2000 and 2008, respectively.

He studied electrical engineering at the University of Duisburg-Essen. He carried out his diploma work during a stay at the University of California at Los Angeles, Los Angeles, CA, USA. From 2006 to 2008 he was with IMST GmbH, Kamp-Lintfort, Germany, where he worked as an RF Engineer. Since then, he has been a Senior Scientist and a Principal Investigator with the Laboratory for General and Theoretical Electrical Engineering, University of Duisburg-Essen. His general research interests include all aspects of theoretical and applied electromagnetics, currently with a focus on medical applications and on-chip millimeter-wave/THz antennas.

Dr. Rennings has received several awards, including the Student Paper Price at the 2005 IEEE Antennas and Propagation Society International Symposium and the VDE-Promotionspreis 2009 for his dissertation.

Daniel Erni (Member, IEEE) received the Diploma degree in electrical engineering from the University of Applied Sciences Rapperswil (OST), Rapperswil, Switzerland, in 1986, and the Diploma degree in electrical engineering and the Ph.D. degree in laser physics from ETH Zürich, Zürich, Switzerland, in 1990 and 1996, respectively.

Since 1990, he has been with the Laboratory for Electromagnetic Fields and Microwave Electronics (IFH), ETH Zürich. From 1995 to 2006, he was the Founder and the Head of the Communication Photonics Group, ETH Zürich. Since October 2006, he has been a Full Professor with the Department of General and Theoretical Electrical Engineering, University of Duisburg-Essen, Duisburg, Germany. He is currently a member of the Center for Nanointegration Duisburg-Essen (CENIDE), University of Duisburg-Essen. In 2017/2018, he joined the Institute of Electromagnetic Fields (IEF), ETH Zürich, as a Visiting Professor. He is also the Co-Founder of the spin-off company airCode, Duisburg, working on flexible printed RFID technology. His current research interests include optical interconnects, nanophotonics, plasmonics, ultrasensitive optical biosensing, advanced solar cell concepts, optical and electromagnetic metamaterials, RF, mm-wave and THz engineering, chipless flexible RFIDs, biomedical engineering, bioelectromagnetics, marine electromagnetics, computational electromagnetics, multiscale and multiphysics modeling, numerical structural optimization, and science and technology studies (STS).

Dr. Erni is a fellow of the Electromagnetics Academy. He is also a member of Materials Chain, the Flagship Program of the University Alliance Ruhr, Electrosuisse, the Swiss Physical Society (SPS), the German Physical Society (DPG), and the Optical Society of America (Optica).